Sensitivity of predictions in an effective model − application to the chiral critical end point position in the Nambu–Jona-Lasinio model[*]

Alexandre Biguet[1], Hubert Hansen[1], Pedro Costa[2], Pierre Borgnat[3], and Timothée Brugière[1]

[1] Institut de Physique Nucléaire de Lyon, CNRS/IN2P3, Université Claude Bernard de Lyon, 69622 Villeurbanne Cedex, France
[2] Centro de Física Computacional, Departamento de Física, Universidade de Coimbra, P-3004-516 Coimbra, Portugal
[3] Laboratoire de Physique, CNRS, l'École normale supérieure de Lyon, 46, allée d'Italie 69364 Lyon cedex 07 France

Abstract The measurement of the position of the chiral critical end point (CEP) in the QCD phase diagram is under debate. While it is possible to predict its position by using effective models specifically built to reproduce some of the features of the underlying theory (QCD), the quality of the predictions (*e.g.*, the CEP position) obtained by such effective models, depends on whether solving the model equations constitute a well- or ill-posed inverse problem. Considering these predictions as being inverse problems provides tools to evaluate if the problem is ill-conditioned, meaning that infinitesimal variations of the inputs of the model can cause comparatively large variations of the predictions. If it is ill-conditioned, it has major consequences because of finite variations that could come from experimental and/or theoretical errors.

In the following, we shall apply such a reasoning on the predictions of a particular Nambu–Jona-Lasinio model within the mean field + ring approximations, with special attention to the prediction of the chiral CEP position in the $(T - \mu)$ plane. We find that the problem is ill-conditioned (*i.e.* very sensitive to input variations) for the T-coordinate of the CEP, whereas, it is well-posed for the μ-coordinate of the CEP. As a consequence, when the chiral condensate varies in a 10 MeV range, μ_{CEP} varies far less.

As an illustration to understand how problematic this could be, we show that the main consequence when taking into account finite variation of the inputs, is that the existence of the CEP itself cannot be predicted anymore: for a deviation as low as 0.6 % with respect to vacuum phenomenology (well within the estimation of the first correction to the ring approximation) the CEP may or may not exist.

PACS. XX.XX.XX No PACS code given

1 Introduction

The critical end point (CEP) was proposed at the end of the eighties [1] and is still a very important subject of discussion nowadays: at finite temperature and chemical potential the most common phase diagram shows a first-order chiral phase transition separating the hadronic phase from the quark phase; this first-order line finishes at the CEP where the phase transition is of second-order and, as T increases and μ decreases, the phase transition becomes a crossover.

The existence of the CEP is still an open problem for theoretical studies based on QCD while its experimental search is in progress [2–10].

Due to its relevance for the QCD phase diagram the search for the CEP becomes one important issue for the heavy ion collision (HIC) program [7–9]: the search of the CEP and the deconfinement transition [7–9] is being undertaken in SPS at CERN [10], in RHIC at BNL [2–4], and in the future facilities FAIR at GSI and NICA at JIRN [11]. The eventual confirmation of the CEP existence would be one of the first QCD-like observables in the medium to be discovered with important implications on the constraint of several effective models.

From the theoretical point of view the existence of the CEP is not consensual: even if older results from lattice QCD [12] predict the existence of the CEP, once the transition is a crossover at vanishing chemical potential, $\mu = 0$, [13,14] it is possible that it may remain of this type also at $\mu \neq 0$. Most of the effective models like the Nambu–Jona-Lasinio (NJL) and Polyakov-loop Nambu–Jona-Lasinio (PNJL) models [15–23] and the Polyakov-loop-improved quark-meson (PQM) model [24,25] also present a first order chiral phase transition that ends at the CEP. However, each model has its own value for the

location of the CEP that depends, for example, on the chosen parametrization [22], on the strength of the vector meson coupling and on the anomaly strength through the 't Hooft coupling constant [26], as well as on the Polyakov-loop. This led to several attempts to constrain some models in order to understand if the CEP exists or not [27–29] namely by fixing the vector meson coupling so that the slope of the pseudo-critical temperature obtained in lattice QCD simulations [30] at small μ is reproduced [27]. Another possible constraint is by showing the existence of a first order QCD phase transition in compact star interiors which lead to the evidence of a first order transition that would prove the existence of at least one CEP in the QCD phase diagram [31].

To better understand the physical mechanism that generates a CEP, one usual approach is to vary some parameters of an effective model to see if the physics controlled by those parameters is relevant to the CEP position prediction. When doing such studies (*e.g.* [22]) we realize the need to have a more systematic and a more quantitative way to proceed. We also realized that instead of varying parameters independently it would be better to vary them in such a way that the inputs phenomenology (used to constrain the parameter in the first place) remains almost constant.

In this paper we develop a method to study some aspects of the sensitivity of a specific NJL model we are studying, that relies on methods used for inverse problems [32,33]. Simply put, an inverse problem consists in finding the model parametrization best reproducing some input data. This can be achieved, for example, by minimizing some merit function as a χ^2 or –as it is the case here– by an exact inversion of the problem. Still, considering it as an inverse problem is by far richer, because it is a framework aiming at extracting and characterizing as much information as possible from the data and their modelization [32]. Note that inverse problem is currently considered as a nice framework of study in the nuclear physics community (*e.g.* [34, 34–37]). Especially, the guidelines described in [34] were particularly interesting and inspiring to develop our work.

For effective models such as the one we will study, related works have shown some deep consequences of the idea that one is solving an inverse problem. In [37], with a framework different from the one presented here, it is shown that varying individually the model parameters may be "misleading and ill advised" to determine the uniqueness of a model if the inverse problem is not well posed. In [36], the relevance of a systematic analysis of the parameter space is discussed. These both works [36, 37] stress that, if the value of the merit function (χ^2 therein) at minimum is a measure of how well the resulting parametrization is able to reproduced the input data, there are other meaningful information to obtain. The curvature around this minimum is one, assessing if the model gives stable and meaningful prediction. Therefore, it is important not to get "trapped in the χ^2 minimum" and to study variations around the minimum so as to get access to the speed at which the χ^2 value deteriorate.

After the parameters fixing, one central question in using an effective model is to estimate if it is reasonable to extrapolate it away of the region where parameters has been fixed, if it keeps its predictive power and how far. For this work, an effective model means the model Lagrangian with the addition of the input parameters, its approximations and the way the parameters are computed. For example, if some in-vacuum inputs are used, one usually assumes that meaningful results can be get at finite temperature (it is indeed one of the earliest successes of the NJL model to show that the quark condensate melts with temperature); yet this remains to be evaluated.

In the present work, a sensitivity parameter is introduced as a way to qualitatively estimate if a prediction is very sensitive to the input (hence there is strong possibility that the predicted value cannot be trusted) or if there is a reason to believe that the prediction is well constrained by the model calculations and the chosen inputs. We will say that in the former case the prediction is unstable (against variation of the inputs) and in the latter that the prediction is stable.

This type of sensitivity analysis is quite common in nuclear theory [34, 38]. However, the precise definition of a sensitivity parameter varies from work to work, although they all estimate how stable a model prediction is. Here, the inverse problem that will be considered has an exact solution (if we where to define a χ^2, its minimum value would be zero) whereas in the aforementioned work the parameters fit is not exact ($\chi^2 \neq 0$). More precisely we will define a sensitivity parameter that measure how an infinitesimal variation of the inputs of the model will impact the value of a prediction.

We found out that the sensitivity parameter that we define later on is very closely related to a criterion defined in the computer science community to estimate if the result of a numerical computation will be damage because real numbers has to be approximated as float numbers (propagation of round-off error) [39]. The sensitivity parameter is indeed related to the so called condition number [40] and is an estimation of the distance between the problem at hand (for example the computation of the solution of a linear system) and the closest ill-posed problem (in that example it would be a non-invertible system). When the condition number is large, the problem is said to be ill-conditioned in the sense that small errors in the data will results in large error in the outcomes.

The proposed reasoning with inverse problems and the associated tool may be quite involved. Since, up to our knowledge, they have not been used widely in the study of the phase of QCD, we will present here a simple analysis based only on the sensitivity parameter and a correlation analysis that was inspired among other works by [34]. We choose the SU(2) NJL model with interaction in the scalar channel only, at the mean field + ring approximation. The inputs will be the quark condensate $\langle \bar{q}q \rangle$, the pion mass m_π and its decay constant f_π. We choose this model because it is good enough to reproduce basic chiral properties of QCD (dynamical mass generation via the spontaneous breaking of chiral symmetry and a

possible CEP) but simple enough to be able to exactly solve the inverse problem and doing part of the calculation semi-analytically. The simplicity of the model and its strong symmetry properties enable us to concentrate on discussing the usefulness of this analysis, to better understand the role of the sensitivity and check the validity of our computation. Even with such simplification we obtain useful results on one key observable of the QCD phase diagram, namely the CEP position.

The paper is organized as follow:
In the first part we will introduce the NJL model and quickly review its relevant phenomenology for this work (spontaneous chiral symmetry breaking, pion properties and the chiral critical end point).
Then we will define the sensitivity parameter, compute its value in the NJL model for several predictions (the sigma meson mass and the pion-quark-antiquark effective coupling constant in vacuum together with the position of the chiral CEP in the $(T - \mu)$ plane) and discuss its relevance to characterize the well- and ill-posedness of the problem.
We will also present an analysis of the situation when one relaxes one of the constraint of the model, namely the value of the quark condensate.
In the second part, the consequences of the previous study will be discussed when finite variation of the fitting data, m_π, f_π and $\langle \bar{q}q \rangle$ are considered. It will illustrate that if the sensitivity analysis may seems fairly abstract, for low value of the dispersion that are well within the expected range of the correction generated by using a next to leading order approximation, the physics can drastically change (namely the CEP may disappear).

2 Sensitivity of predictions of the Nambu–Jona-Lasinio model

2.1 Parametrization of the Nambu–Jona-Lasinio model; observables

We consider the local two flavor NJL model in $SU(2)$-isospin approximation whose Lagrangian is (see [41–44] for reviews):

$$\mathcal{L}_{NJL} = \bar{\psi}(i\gamma^\mu \partial_\mu - m_0)\psi + G\left[(\bar{\psi}\psi)^2 + (\bar{\psi}i\gamma_5 \boldsymbol{\tau}\psi)^2\right] . \quad (1)$$

This Lagrangian depends on three dimensional parameters, m_0 the bare quark mass of the u and d quarks in SU(2)-isospin approximation (in GeV); G the coupling constant (GeV^{-2}) and Λ the three-dimensional cutoff mimicking the asymptotic freedom of quarks (in GeV). Since the NJL model cannot be extracted directly from QCD, they are free parameters, but, nevertheless, they are loosely constrained: m_0 should be of the order of the masses of u and d quarks, Λ is related to the scale Λ_{QCD}; for what concern G if one think of it as the Fermi coupling in the electroweak theory, $G \simeq g/M^2 \simeq \tilde{g}/\Lambda^2$, then $\tilde{g}$ is poorly constrained but is usually expected to be in a range [1, 10].

These parameters are usually fitted to the values of the pion mass, m_π, the pion decay constant f_π, and the quark condensate $c = -\langle \bar{q}q \rangle^{1/3}$ normalized to be positive and with the dimension of an energy. The latter quantity is related to the so-called dressed quark mass m that cannot be considered as an observable but provides a physical picture of the hadronic world after the spontaneous chiral symmetry breaking in terms of quasi-particles with $m \gg m_0$ and also a very crude approximation of the nucleon mass as 3 times the mass of one dressed quark.

The scheme we choose to compute those quantities is the mean field approximation for the condensate and the ring approximation for the meson properties [41].
For the mean field effective quark mass $m(\Lambda, m_0, G)$ one has the so-called gap equation:

$$m_0 - m + 8iGN_cN_f mI_1 = 0 \quad (2)$$

where I_1 is the 1-propagator line integral that arises from the tadpole diagram:

$$I_1 = -i \int^\Lambda \frac{\mathrm{d}^3p}{(2\pi)^3} \frac{1}{2E_p} \text{ (with } E_p^2 = p^2 + m^2). \quad (3)$$

Then the mean field quark condensate $\langle \bar{q}q \rangle(\Lambda, m_0, G)$ is:

$$\langle \bar{q}q \rangle = \frac{m_0 - m}{2G} . \quad (4)$$

Finally $m_\pi(\Lambda, m_0, G)$ and $f_\pi(\Lambda, m_0, G)$ are given by:

$$m_\pi^2 = -\frac{m_0}{m} \frac{1}{4iGN_cN_f I_2(0)} , \quad (5)$$

$$f_\pi^2 = -4iN_c m^2 I_2(0) , \quad (6)$$

where I_2 is the 2-propagator lines integral coming from the quark loop diagram of the ring approximation ; we also use a quasi-Goldstone boson approximation assuming the pion mass can be neglected, namely the argument of I_2 is $k^2 = 0$ and not $k^2 = m_\pi^2$. Explicitly one has:

$$I_2(0) = -i \int^\Lambda \frac{\mathrm{d}^3p}{(2\pi)^3} \frac{1}{4E_p^3}. \quad (7)$$

When $(m_\pi, f_\pi, \langle \bar{q}q \rangle)$ are fixed to their phenomenological values, the inverse problem is solved when the system:

$$m_\pi(\Lambda, m_0, G) = m_\pi , \quad (8)$$

$$f_\pi(\Lambda, m_0, G) = f_\pi , \quad (9)$$

$$\langle \bar{q}q \rangle(\Lambda, m_0, G) = \langle \bar{q}q \rangle , \quad (10)$$

is solved for the parameters Λ, m_0 and G. Thanks to the quasi-Goldstone approximation this system has quasi-analytic solutions discussed in App. (A). As we show in this appendix, the previous system has solutions only if the ratio $\alpha = f_\pi^3/\langle \bar{q}q \rangle$ is greater than a constant critical value (it is related to the discussion in Sec. 2.2.2 of [43]). Among the solutions, only one is physical.

When parameters are fixed, this NJL model can describe some simple phenomenology in vacuum as the sigma meson mass m_σ and the pion-quark coupling constant $g_{\pi\bar{q}q}$ (see [41] for details):

$$m_\sigma = \sqrt{4m^2 + m_\pi^2}\,,$$
$$g_{\pi\bar{q}q} = \frac{1}{\sqrt{-4iN_c I_2(0)}}\,. \qquad (11)$$

The NJL model is also able to predict, for a range of parameters, a first order transition toward a phase where the chiral symmetry is partially restored. At the end of this line there is a critical end point in the $(T-\mu)$ plane whose properties are described in App. (B) (we also describe a new very fast and stable algorithm to compute it).

2.2 Sensitivity and ill-posedness of a problem

To study the sensitivity of a given prediction we will use a condition number [40] of the problem: it is a local measure (based on a gradient calculation) of the sensitivity of a solution to this problem against infinitesimal variation of its inputs. Here we will use the relative condition number: when it is infinite, the problem is ill-posed; when it is finite but large (compared to one) the problem is said ill-conditioned.

The choice we made to compute it is based on the statistical propagation of errors because it is a natural way to compute the variation (the standard deviation) of an output with respect to input variations that are supposed uncorrelated when one minimizing a χ^2 (as we will do in the future where an exact inversion is not possible) and for the correlation analysis.

Let X be a prediction depending on two inputs a and b: the standard deviation of a prediction X is computed by propagating the variation $\sigma(a)$ and $\sigma(b)$ of the parameters:

$$\sigma^2(X) = \left(\frac{\partial X}{\partial a}\right)^2 \sigma^2(a) + \left(\frac{\partial X}{\partial b}\right)^2 \sigma^2(b)\,. \qquad (12)$$

The sensitivity is the ratio of the relative standard deviation and the mean of the relative variation of the inputs:

$$\Sigma(X) = \lim_{\sigma \to 0} \frac{\sigma_{rel}(X)}{\sigma_{rel}^I} \qquad (13)$$

where,

$$\sigma_{rel}(X) = \frac{\sigma(X)}{X} \qquad (14)$$

$$\sigma_{rel}^I = \frac{1}{2}\left(\frac{\sigma(a)}{a} + \frac{\sigma(b)}{b}\right)\,, \qquad (15)$$

and $\lim_{\sigma \to 0}$ means we take infinitesimal variations of the inputs. The way one takes this limit has to be specified. We choose to take vanishing *relative dispersion* of the inputs namely for $I = a$ or b, $\sigma(I)/I = p$ and $p \to 0$. We will briefly discuss another choice (to cross check our results),

the vanishing *absolute dispersion* case, where if all inputs have the same dimension, $\sigma(I) = d$ and $d \to 0$.

Explicitly with the relative dispersion and for the inputs (m_π, f_π, c) we have:

$$\Sigma(X) = \sqrt{\left(\frac{\partial X}{\partial m_\pi}\right)^2 \frac{m_\pi^2}{X^2} + \left(\frac{\partial X}{\partial f_\pi}\right)^2 \frac{f_\pi^2}{X^2} + \left(\frac{\partial X}{\partial c}\right)^2 \frac{c^2}{X^2}}\,, \qquad (16)$$

where it can be noticed that:

$$\left(\frac{\partial X}{\partial a}\frac{a}{X}\right)^2 = \left(\frac{\partial \ln X}{\partial \ln a}\right)^2\,. \qquad (17)$$

In the rest of this paper we will argue that if the sensitivity of a prediction is large (the calculation is ill-conditioned) it means that it cannot be trusted and should be excluded because any small but finite errors in the inputs (either measurement errors as for the condensate or theoretical errors because of the approximations) will have a great chance of damaging the prediction. We will say that the prediction is unstable.

On the contrary, a prediction with a small sensitivity can be trusted in the context of the particular model used to predict it. The physics that has been used to write the model and the chosen inputs are enough to give a stable, well constrained prediction.

In our work, we choose to use a model describing the chiral physics where spontaneous chiral symmetry breaking is generated only by the scalar interaction and the inputs are related to this physics: the pion properties (the quasi-Goldstone boson of this mechanism whose mass and decay constant are related via the PCAC) and the non vanishing chiral condensate.

We will illustrate the use of the sensitivity with 3 cases: stable prediction in vacuum, stable and unstable prediction in medium at zero and finite dispersion.

2.2.1 A remark on the sensitivity calculation: Monte Carlo setup

It is in principle possible to compute the sensitivity analytically. In the present context this can actually be done quite easily for the in-vacuum predictions because the inverse problem is exact. Details of the calculation of $\Sigma(m_\sigma)$ can be found in App. (C). In the simple model we considered, the calculation of $\Sigma(T_{\mathrm{CEP}})$ and $\Sigma(\mu_{\mathrm{CEP}})$ is still treatable, but more complicated because it requires to compute the derivatives of a system of three implicit equations (see App. (B)). The calculation of these derivatives will become even more complicated (for example the dimensionality of the system will increase) when more realistic model, with vector channel interactions or with the Polyakov loop, will be used.

If we choose this particular model it is precisely because of its simplicity hence besides some results relevant for the physics of the CEP, this work is also a benchmark for further studies: in this model we are able to cross check analytically large part of our numerical results.

For this reason we choose to compute the sensitivity using a Monte-Carlo setup. It has the advantage that for higher dimensionality of the CEP system (thus for more realistic model) it is well known a Monte-Carlo will nicely scale whereas an analytic calculation would become uninteresting (it is common that analytic derivatives formula are not well suited for a computation because of differences or ratio of almost identical terms) and a numerical calculation could become too time consuming (it is the famous problem of equidistant sampling versus random sampling in a high dimensionality space).

Besides, since we use the statistical error propagation formula, the Monte Carlo is a natural framework to compute mean and standard deviation. The last advantage of Monte Carlo at non vanishing dispersion is the fact that one can visualize the data and have a better understanding of the dispersion pattern of the CEP or the correlations (as it will be discuss in the last section).

The details of the Monte-Carlo setup are only relevant in the case of a finite dispersion of the inputs; they will be discuss there.

2.3 Results on the sensitivity of some NJL predictions

Let us come to the first results of this work.
We choose the following value for the inputs:

$$\begin{pmatrix} m_\pi \\ f_\pi \\ \langle \bar{q}q \rangle^{1/3} \end{pmatrix} = \begin{pmatrix} 137 & \text{MeV} \\ 93 & \text{MeV} \\ -315\,\text{MeV} \end{pmatrix} . \qquad (18)$$

The value for the quark condensate is equivalent to choose the u condensate as $\langle \bar{u}u \rangle^{1/3} \simeq -250$ MeV. Such value is in agreement with limits extracted from sum rules, $190\,\text{MeV} \le -\langle \bar{u}u \rangle^{1/3} \le 260$ MeV at a renormalization scale of 1 GeV [45], and $\langle \bar{u}u \rangle^{1/3} = -270$ MeV at a renormalization scale of 2 GeV [46]. This value is also in agreement with recent result of lattice calculations: $\langle \bar{u}u \rangle^{1/3} = -269(08)$ MeV [47].

2.3.1 Parametrization

In our context the true inputs of the model are the phenomenological observables m_π, f_π and $\langle \bar{q}q \rangle$ from which the physical parameters are uniquely defined. So the model parameters also have a sensitivity. As noticed by [36,37], a variation around the solution of the inverse problem also contains information on the accuracy of the model. Very large sensitivity would mean that from the very beginning the model cannot be used to do predictions because the whole model itself (and not one of its predictions) is ill-conditioned (let us recall that by model we mean the Lagrangian, its approximation and also its inputs). We will see in the section 2.4 a case where $\alpha \to \alpha_c$ (α_c is the limit value of $f_\pi^3/\langle \bar{q}q \rangle$ where the inverse problem cannot be solve anymore, see App. (A)): all sensitivities diverge at that point, even the parameters one. At this specific point, the model in itself becomes ill-posed and nothing

can be done with it. A correlation analysis would also be interesting: very low correlation of the parameters with the inputs would be a signal that the chosen inputs are not the relevant ones to constrain the parameters [37].

In Tab. 1 one can read that we are rather safe with the parametrization, the magnitude of sensitivities being below 5.

It is worth noticing that a symmetry relation provide us a very easy way to compute $\Sigma(m_0)$ but also to get more information. An approximate value is easily obtained: at first order in the bare mass m_0 the GMOR relation $m_\pi^2 f_\pi^2 = -m_0 \langle \bar{q}q \rangle$ leads to $dm_0/m_0 = 2dm_\pi/m_\pi + 2df_\pi/f_\pi - 3dc/c$ hence $\Sigma(m_0) = \sqrt{17} = 4.12$. By writing the differential we see that the m_0 sensitivity is decomposed in 3 almost equal source terms for the sensitivity (namely the 3 logarithmic derivatives). From this decomposition one can learn that m_0 will be almost equally sensitive to variations of any of the inputs. By the examination of Eq. (25) it is not obvious at first glance that this should be the case. One could think that m_0 is strongly sensitive to m_π but due to the GMOR relation it is not the case. Then, even at the simplest level, we think that the study of sensitivities with respect to the inputs and their sources (related to the partial derivative) can bring information that may be difficult to find based on purely physical argument. For the case of m_0 the GMOR relation is enough to reveal the hidden link between observables but we will see that the more complicated the prediction, the less obvious this kind of link can be found without a sensitivity calculation.

Finally let us stress again the first strong strength of a sensitivity analysis: if the sensitivities of the parameters are large it is meaningless to even try to use the model.

	Sensitivities		Values
Parameters	Λ	2.83	0.653 (GeV)
	m_0	4.11	0.0051 (GeV)
	$G\Lambda^2$	3.32	2.11
In-vacuum predictions	m	6.72	0.313 (GeV)
	m_σ	6.41	0.642 (GeV)
	$g_{\pi\bar{q}q}$	5.97	3.37
In-medium predictions	T_{CEP}	71.5	0.0299 (GeV)
	μ_{CEP}	1.05	0.327 (GeV)

Table 1. Sensitivities of the parameters, in-vacuum predictions and in-medium predictions considering infinitesimal changes of the inputs. The sensitivities of the parameters, of the in-vacuum predictions and of μ_{CEP} are close to 1. The sensitivity of the temperature coordinate of the CEP is very large. These values were computed numerically with a Monte-Carlo.

2.3.2 Prediction sensitivities

Considering that our model is constrained in vacuum, in Tab. 1 we organize the sensitivities (top to bottom) from the expected lowest values (for the parameters) to the expected greatest values (for the in-medium predictions).

We began our discussion on the usefulness of the sensitivity analysis by the sigma meson mass and the pion-quark-antiquark effective coupling constant in vacuum (see Eq. (11)).

As expected, the sensitivities of the in-vacuum predictions are larger than the one of the parameters, but are still not too large (< 7). The phenomenological conclusions that can be done within this model in the in-vacuum mesonic sector are rather safe.

Let us take a closer look on the sigma mass: In App. (C) we compute analytically $\Sigma(m_\sigma)$ (hence checking that the present Monte Carlo setup is correct) and obtain the result for the differential $\mathrm{d}m_\sigma = 0.21\mathrm{d}m_\pi + 34\mathrm{d}f_\pi - 8.2\mathrm{d}c$. First of all we see that the sensitivity coming from the pion mass partial derivative is negligible and this is not surprising: it is well known that the Goldstone theorem is approximately realized in NJL due to the the small values of the bare quark mass so the sigma mass is essentially twice the dressed quark mass. In fact, for this reason all observables are barely sensitive to the pion mass (except of course if they correlate directly with m_0).
But the sensitivity analysis can show relations that are more difficult to predict based on simple symmetry arguments. For example, since $m_\sigma^2 = 4m^2 + m_\pi^2$ and since m is essentially due to the chiral symmetry breaking in the NJL model by a quick examination of the equation one could have expected that the sigma is mainly sensitive to the condensate variation. The coefficients of this differential shows that it is also sensitive to f_π a fact that is not easily read in the NJL model due to the non-linear relation between the scale Λ, f_π and the condensate. Let us stress again that this simple model is used as an illustration of the usefulness of this technique; the link between observables may not be apparent by examination of the NJL equations but for the specific case of f_π one can see for example in a linear sigma model that the PCAC imposes an approximate proportionality between the vacuum expectation value of the sigma field and f_π: $v^2 = f_\pi^2(1 + o(m_\pi^2))$ hence a strong correlation between m and f_π. It is another example of the fact that sensitivity or correlation analysis can bring to light such relations, hidden by the non linearity of the equations. For the CEP, such correlations become very difficult to predict a priori (as we will see in the following) hence the analysis is a useful one for phenomenology.

Finally let us conclude by examining the sensitivities of the in-medium predictions of T_{CEP} and μ_{CEP}. They are both surprising. On the one hand the sensitivity of the T-coordinate of the CEP is very large (~ 70) and the one of the μ-coordinate is very close to 1, even more close than the sensitivities of the model parameters.
Concerning the T_{CEP}, the conclusion is quite easy. The model, that consists of the approximation schemes and of the phenomenological inputs, is ill-conditioned for the prediction of the temperature coordinate of the chiral CEP: we try to push too far the model from the vacuum where its parameters are constrained. This means that no consistent conclusions can be drawn concerning T_{CEP} in this

context (we will detail this in the section devoted to small but finite variation of inputs).
The conclusion is completely different for μ_{CEP}. Its close to unity sensitivity means that the physics that is implemented in this simple NJL model, i.e. chiral symmetry and scalar sector, is part of the physics that constrains the chemical potential coordinate of the CEP. This does not mean that the μ_{CEP} in nature is the one that is predicted by this NJL model but this means that the chiral physics generated by the scalar channel seems to be very relevant to this prediction. For example adding new physical contents to the model, such as vector channel interactions, will certainly change the position of μ_{CEP} in the phase diagram (essentially it will shift it [41]) but we have reason to believe it will not alter drastically the sensitivity of μ_{CEP} and not solve the sensitivity problem of T_{CEP}[1]. To solve this problem one probably need in-medium constraints as we will check in a future work.

2.4 Sensitivities for different values of the quark condensate

Since the value of the quark condensate is less well known when compared to the pion mass and the pion decay constant, we plot the sensitivities of m, T_{CEP} and μ_{CEP} as a function of the value of the condensate with m_π and f_π fixed to their values given in Eq. (18).

In Fig. (1), the constituent quark mass, the temperature coordinate of the CEP, its chemical potential coordinate and their corresponding sensitivities are plotted as a function of the value of the quark condensate in the range $[306, 316]$ MeV. At $c = 306$ MeV, $\alpha \simeq \alpha_c$ and the inverse problem does not have a solution anymore; at $c \simeq 316$ MeV, $T \simeq 0$: the CEP disappears from the phase diagram. As we mentioned earlier, we see that the sensitivities diverge at the lower limit of the range. It is the case for all quantities: in fact at this point, the model is ill-posed and the parameters cannot even be fixed.

On the lower panel of Fig. (1), one can see that μ_{CEP} only varies in a 2.5 MeV range and this is coherent with what we expect from the behavior of a quantity with such a small sensitivity: the prediction of μ_{CEP} is very stable even with respect to large variation of the condensate (this is also confirmed by our calculation of the correlation of μ_{CEP} with the condensate that turn out to be small as can be seen in Tab. 5 ; correlations will be discussed in the last part). On the contrary the constituent mass varies in a range of 85 MeV (upper panel) and T_{CEP} in a 60 MeV range (middle panel). This is coherent with the fact that m and T_{CEP} have larger sensitivities. As a side note, we see that $\Sigma(T)$ is large on the whole interval signaling a fundamental problem for this model in order to constrain the temperature and give an accurate prediction; also it even diverges just before the CEP disappears.
On this range $\Delta m/m \simeq \pm 11\%$ and $\Delta T/T \simeq \pm 100\%$. Of

---

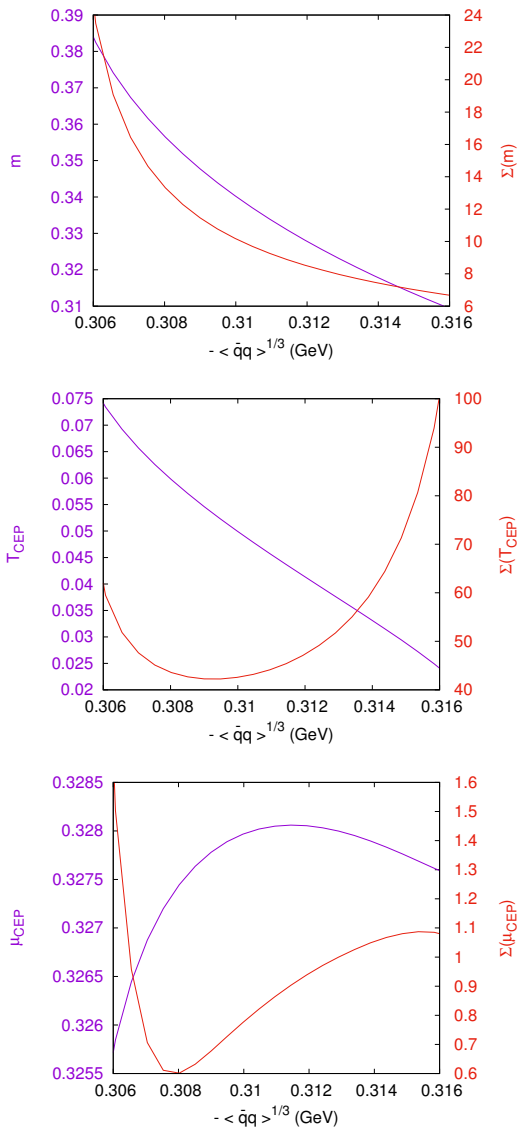[1] This conjecture is based on [48] Fig. 1 where the CEP seems to remain not very well constrained.

Figure 1. The constituent quark mass m (top), the temperature coordinate of the CEP (middle) and the chemical potential coordinate of the CEP (bottom) as well as their corresponding sensitivities are plotted as functions of $-\langle \bar{q}q \rangle^{1/3}$. We limit the range of the quark condensate such that the inverse problem always has a solution and that the CEP always exists. When the quark condensate varies in a 10 MeV range, the constituent quark mass varies in a 85 MeV range, T_{CEP} varies in a 60 MeV range and μ_{CEP} only in a 2.5 MeV range. These windows are closely related to the values of the sensitivities that are average for m, large for T_{CEP} and close to 1 for μ_{CEP}

course these values are not exactly the sensitivities previously computed. Sensitivities are local quantities (related to a gradient with respect to the 3 directions in the inputs space) but it shows that there is a correct agreement between this finite variation and an extrapolation based on the first order of a Taylor expansion (whose coefficient is related to the sensitivity). It shows that the problem is sufficiently linear (at least in the c direction) around

the input values for the sensitivity to be a useful quantities even in this non linear problem. We will use this fact when studying finite variations of all 3 parameters.

Since the quark condensate is closely related to the dynamical generation of the mass and the latter being a relevant phenomenon for the creation of a first order phase transition at zero temperature we could anticipate that μ_{CEP} and m would varies accordingly when $\langle \bar{q}q \rangle$ only is varied. By comparing the upper and lower panels, one can see it is not the case: the larger sensitivity of the constituent mass leads to a large variation of the mass but the chemical potential is remarkably stable. This result shows how the non-linearity of the inverse problem may affect the outcome in a non trivial way that is revealed by the sensitivity. We will see that the chemical potential is strongly correlated with the pion decay constant.

From top of Fig. (1), one notices that, at fixed f_π and m_π, the constituent quark mass reduces when c raises. From $m \simeq 2Gc^3$, one could expect that m would increase when c increases, and so should μ_{CEP} since it would take more density to destroy the condensate. Here, the calculation results in a decrease of m while μ_{CEP} is non-monotonic. This is another interest of varying the inputs of the model and not the model parameters: the phenomenology may vary counter intuitively when one realizes that the true inputs are the datae. In fact, when m_π and f_π are fixed, $G \equiv G(\langle \bar{q}q \rangle)$, and then $m \simeq -2G(\langle \bar{q}q \rangle)\langle \bar{q}q \rangle$, and the non linear behavior of G makes wrong the first conclusion.

Finally, let us recall that this analysis is rooted in the nuclear physics community (both theory and experiments). It can serve as a guide for experiments. As noticed by [37] the correlation analysis can almost systematically determines which observables are the best to provide constraints on parameters and then experiments can concentrate on the most readily accessible of these observables. In our case and as a though experiment, let us suppose one moment that the scalar channel is the only relevant one, that the CEP has been shown to exist (for example if it is shown that at zero temperature in compact star phenomenology the chiral transition is first order) and the pion properties are well known but the chiral condensate has not been measured. The result of this section shows that the chiral condensate must be searched in the range [306, 316] MeV even if we cannot point where the CEP should be in the phase diagram due to the temperature sensitivity.

2.4.1 On the choice of the dispersion pattern

We have chosen to take equal relative dispersion of the inputs. Of course choosing equal absolute dispersion changes the results. With the values we use for the inputs it means that the condensate varies approximately 3 times more that the other inputs. It can be an informed choice, for example if one estimates that since it is less known it should vary more. In any way to check if our conclusion where change by this choice we also computed with absolute dispersion. None of the above conclusions are changed by the other choice.

3 Consequences of small but finite deviations of the inputs

3.1 Why finite variations are relevant

In our case of an exact inverse problem a large value of $\Sigma(T)$, that is a calculation close to a ill-posed one, may be harmless since it is computed at vanishing dispersion and the parameters fixing procedure is exact. Indeed, if the inputs are very accurately computed in the model and very well measured, the outcome may vary only slightly (the situation would be worse if we used a $\chi^2 \neq 0$ to parametrize the model since there would be no way to fix the parameter to reproduce the exact inputs). However, as an illustration of our previous analysis we will show that for our calculation of the CEP it is unacceptable. We will see that very small variations (0.6%) around the vacuum will already completely change the physics of the model, namely with such small variations the CEP may or may not exists. The problem is that the inputs are neither very well measured nor accurately computed.

On the one hand the quark condensate value is not very well known as explained earlier. On the other hand let us stress that when we compute the sensitivity in this model we mean the NJL Lagrangian and also its approximations. By comparing our results with results obtained with a less approximate treatment we can evaluate roughly the order of magnitude of the systematic errors generated by the approximation.

For example, relaxing the quasi-Goldstone boson approximation (we reinstate $k^2 = m_\pi^2$ in Eq. (5)) we find $m_\pi = 135.6$ MeV accounting for a variation of about 1%.

Let us consider the next order in a $1/N_c$ expansion as the meson-loop approximation (MLA) [49]. In this work, the correction on the pion properties were found around 5% (the value depending on details of the model calculation). In the framework of the inverse problem, it means a re-parametrization has to be made to get back the correct vacuum phenomenology. Here we do the assumption that, during the re-parametrization procedure, the previously computed mean field sensitivity may already generate a variation for a prediction X of about $\Sigma(X) \times 5\%$.

We believe that our calculation of the sensitivity and a rough approximation of the contribution of the next order, for the inputs, is able to determine if this correction will be likely to damage the current calculation.

3.2 CEP unpredictability

In order to see the concrete effects of large or small sensitivities of the predictions, we allow the phenomenological inputs to vary in a small range given by a relative dispersion $p = 1\%$ of the mean values given in Eq. (18). As we have seen this value is rather conservative considering the MLA estimation. It is worth writing explicitly the range where our value will fluctuate. The range is rather small (especially when looking to various NJL model parametrization in the literature) and yet the physics will be completely changed:

$$
\begin{array}{rcl}
m_\pi & \in & [\ 135.6 \ , \ 138.4 \ ] \\
f_\pi & \in & [\ 92.07 \ , \ 93.93 \ ] \\
\langle \bar{q}q \rangle^{1/3} & \in & [-318.1 \ , \ -311.8 \ ]
\end{array}
\tag{19}
$$

We will then see if the value of the sensitivities has a consequence on the prediction with finite dispersion. Also additional information can be acquired. The shape of the distribution, for example of the CEP in the $(T - \mu)$ plane, can now be visualized, together with correlation plots.

We must now explain precisely our Monte Carlo setup (the previous calculation were done in the exact same way with $p = 0.005\%$ and we checked that it was small enough for the calculations to extrapolate toward $p = 0$).
A set of n input points is generated following a given probability density (the choice of the density is irrelevant at vanishing dispersion).

The uniform distribution $\rho^u(X)$, which is suited for analysis of deterministic errors, is a constant around its mean value $\bar{X}$:

$$
\rho^u(X) = \mathcal{N}\theta(X - X_{\max})\theta(X_{\min} - X) ,
\tag{20}
$$

with θ the Heaviside function, $\mathcal{N}$ a constant that normalizes the density to one and where $X_{\min} = (1 - p)\bar{X}$, $X_{\max} = (1 + p)\bar{X}$, where $p = 1\%$.
The Gaussian distribution $\rho^G(X)$ is usually used when supposing a random variable normally distributed with a standard deviation σ. The interest of the Gaussian distribution is that its wings will allow us to explore points that are not in the uniform distribution. To compare the results obtained with the uniform distribution, we used $\sigma = p\bar{X}$ and then:

$$
\rho^G(X) = \mathcal{N}e^{(X - \bar{X})/2\sigma^2} ,
\tag{21}
$$

where again $\mathcal{N}$ is the normalization of the distribution. Using these definitions we checked that the results do not change qualitatively when using the uniform or the Gaussian distribution.

Then, the inverse problem is solved leading to n sets of parameters. For each of these sets of parameters the in-vacuum as well as the in-medium predictions are computed. At the end, distributions for m_σ, $g_{\pi\bar{q}q}$ and also for T_{CEP} and μ_{CEP} are obtained. For each of the distribution ρ_X of the prediction X a mean value $\bar{X}$ and a standard deviation $\sigma(X)$ can be computed. The sensitivity of the prediction X Eq. (16) becomes:

$$
\Sigma(X) = \frac{\sigma(X)}{\bar{X}} \frac{1}{\sigma_{rel}^I} .
\tag{22}
$$

3.2.1 Distributions of the model parameters

The probability distribution of α is plotted in Fig. (2) where the theoretical distribution, that is calculated in App. (D), is also shown as a cross check.
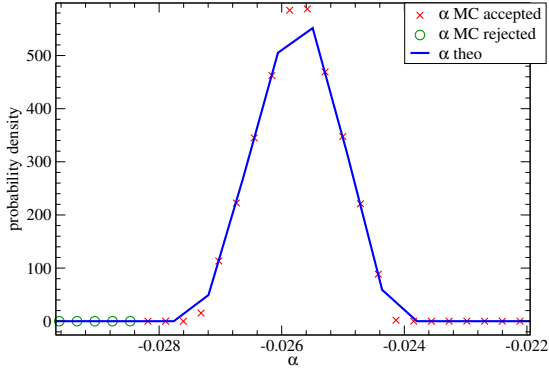
Figure 2. Distributions of α with a dispersion $p = 1\%$ of the inputs for the uniform distributions. The full line represents the theoretical density given by Eq. (100), and the circle and cross are the value of a normalized histogram (the integral is one) obtained with the Monte Carlo simulation ($n = 50^3$). The crosses are the accepted parameters (satisfying $\alpha > \alpha_c$), and the circles are the rejected parameters ($\alpha < \alpha_c$).

In Fig. (3) we plot the obtained distributions of the NJL model parameters. We also represent the mean and standard deviation of the parameters and check that the statistics was large enough to have well controlled errors. For each random variable X, another point is represented on the figures whose error bar are $S(X) = \overline{X} \sigma_{rel}^I$. This point allow us to compare the relative standard deviation of a quantity to σ_{rel}^I. When $\sigma(X) > S(X)$ we have a visual estimation that the chosen dispersion for the inputs results in a larger dispersion for this output. This point is related with the sensitivity, indeed $\Sigma(X) = \sigma(X)/S(X)$.

The bare quark mass value is between 4 and 6 MeV, typical values found in literature. It is worth noticing that with a sensitivity of 4, if one would like to tackle the difficult problem of the evaluation of the bare quark mass with this model and measurements of pion properties and the condensate, the value would be affected by a large uncertainty.

For what concerns G there is a small absolute dispersion of the parameter and one notices a very sharp low cut of its value. The sharp cut induces a strong asymmetry of the density as can be seen from the position of the mean. The values of $G\Lambda^2$ are located around 2.1 with $\sigma(G) \simeq 0.1$.

Finally, Λ displays a quite large standard deviation and its typical values are between 600 and 700 MeV. The latter value is a bit large compared to the usual parametrization of the model.

3.2.2 Distributions of the sigma mass

Fig. (4) presents the distribution of m_σ and its mean value and associated standard deviation. These quantities are also gathered in Tab. 2, with the corresponding values for the other prediction $g_{\pi\bar{q}q}$. We can notice that the shape of the density, even with the sharp cut of the uniform parameter distribution, present a long tail for higher value of the mass, not completely excluding value as high as 800 MeV (the same tail can be seen for $G\Lambda^2$). As we can see
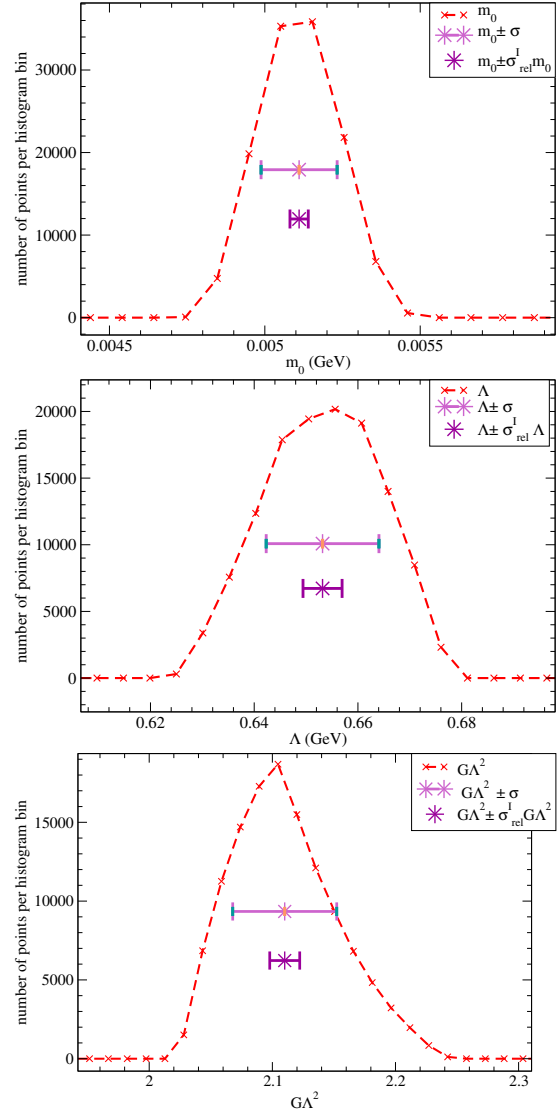

Figure 3. The crossed lines represent the distributions of the dimensional parameters of the NJL model (un-normalized histogram whose integral is the number of points): m_0 (top), Λ (middle) together with $G\Lambda^2$ (bottom). The results are obtained with the Monte Carlo simulation with a variation of 1% of the inputs for the uniform distribution and $n = 50^3$. The top star point and the error bar represent the mean and standard deviation. The bottom star point has error bar whose value is the mean times the standard deviation of the inputs, $S(X) = \overline{X} \sigma_{rel}^I$, a way to visualize the sensitivity of the output with respect to the dispersion of the inputs (see discussion in text). Notice how these error bars are always smaller (especially for m_0) than the standard deviation illustrating how an initial dispersion of the inputs translates in larger deviation of the outputs.

from the table, the results for m_σ and for $g_{\pi\bar{q}q}$ are in accordance with the phenomenology of simple quark models ($m_\sigma \simeq 600$ MeV is the expected value for the sigma mass in this framework; it cannot be compare to the experimental scalar meson as discussed for example in [50,51]).
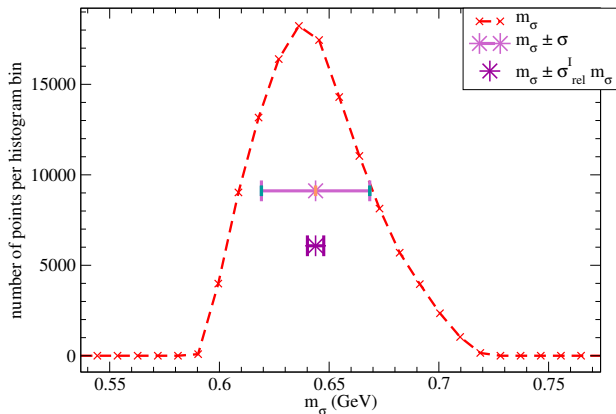
Figure 4. The crossed lines represent the distributions of m_σ (un-normalized histogram whose integral is the number of points) obtained with the Monte-Carlo simulation with variations of 1% of the inputs for the uniform distributions and $n = 50^3$. The top stars and its error bars represent a visualization of the sensitivity (see Fig. (3) and text).

Furthermore, the dispersions of these quantities are reasonable (less than 7%).

$\overline{m_\sigma}$	(0.6439 ± 0.0003) (GeV)
$\sigma(m_\sigma)$	(0.0246 ± 0.0002) (GeV)
$\sigma(m_\sigma)/\overline{m_\sigma}$	3.82 (%)
$\overline{g_{\pi\bar{q}q}}$	3.3822 ± 0.0001
$\sigma(g_{\pi\bar{q}q})$	0.209 ± 0.002
$\sigma(g_{\pi\bar{q}q})/\overline{g_{\pi\bar{q}q}}$	6.18 (%)

Table 2. Results obtained for the in-vacuum predictions m_σ and $g_{\pi\bar{q}q}$, for the uniform distribution, with $n^3 = 50^3$ and $p = 1\%$.

3.2.3 Distribution of the chiral critical end point prediction

Let us come to the most striking result of this section. As explained before, it may happen that the inverse problem has a solution but the corresponding parameter set does not lead to a CEP. With a dispersion as low as 0.6%, the CEP starts to disappear. Hence the sensitivity of the CEP temperature is so large that the prediction is already spoiled if one assumes only 0.6% variations of the inputs. The existence of the CEP (even if it exists when using the mean value of the inputs) cannot be considered as a true prediction of this particular model; the physical outcome of the model is completely changed.

As a reference the number of obtained sets of parameter and the number of calculated CEP for a dispersion of 1% and 0.5% is listed in Tab. 3.

In Fig. (5) we present a scatter plot of the CEPs obtained in this calculation with the confidence ellipses at $1 - \sigma$ and $2 - \sigma$. The confidence ellipses are an approximation of the true $1 - \sigma$ and $2 - \sigma$ confidence level since the density $\rho(T_{CEP}, \mu_{CEP})$ is not a Gaussian distribution.

Uniform distribution			
p (%)	n_{sets}	n_{CEP}	$n_{\text{CEP}}/n_{\text{sets}}$ (%)
1	3375	3066	91
0.5	3375	3375	100

Table 3. From the $n^3 = 15^3$ input sets generated with dispersion p in the Monte-Carlo, n_{sets} parameter sets could be calculated (the solution of the inverse problem exists) and n_{CEP} admit a CEP.

These ellipses are just a convenient way to represent the covariance matrix since the semi-major and semi-minor axis are the eigenvectors of this matrix.

Another noticeable result is that with a dispersion as low as 1% (resulting in at most 3 MeV of variation of the phenomenological inputs of the model) the CEP scatter plot extends in a large range of temperature $T_{\text{CEP}} \in [0, 55]$ MeV and a more reduced range of chemical potential $\mu_{\text{CEP}} \in [324, 332]$ MeV (the standard deviation is of course much smaller). Furthermore, it exists some parameter sets for which a CEP does not exist. For all this sets, the phase transition at $T = 0$ is a crossover. To visualize this feature, a point for the nonexistent CEP is added: its temperature is taken as $T = 0$ (the CEPs disappear "from below") and its chemical potential such that $d\mu/dm = 0$ at $T = 0$[2]. To visualize also the density of the point we represent in Fig. (6) the probability distribution of the CEP using the Kernel Density Estimate or KDE (shortly described in App. (E)). The integral on $\mathbb{R}^2$ of this distribution is one and its dimension is GeV^{-2}.

In Tab. 4 the mean and standard deviation are listed. The ratio of the deviation over the mean of the temperature may seem low compared to the value of the sensitivity. It is an artifact coming from the fact that the "missing CEP" cannot be taken into account hence lowering artificially this ratio. This ratio for the chemical potential is remarkably low.

These results are in agreement with the values of the sensitivities at vanishing dispersion that we found for the CEP. As already noticed, the problem is sufficiently linear around the mean value for the sensitivities calculation to make sense when extrapolated at finite dispersion.

$\overline{T_{\text{CEP}}}$	(0.0303 ± 0.0001) (GeV)
$\sigma(T_{\text{CEP}})$	(0.0107 ± 0.0001) (GeV)
$\sigma(T_{\text{CEP}})/\overline{T_{\text{CEP}}}$	35.25 (%)
$\overline{\mu_{\text{CEP}}}$	(0.3280 ± 0.0001) (GeV)
$\sigma(\mu_{\text{CEP}})$	(0.0018 ± 0.0001) (GeV)
$\sigma(\mu_{\text{CEP}})/\overline{\mu_{\text{CEP}}}$	0.54 (%)

Table 4. Results obtained for the in-medium prediction, i.e concerning the CEP position, for the uniform distribution, with $n^3 = 20^3$, and $p = 1\%$. This analysis does only take into account the CEPs that were find. Thus the presented results are biased. If the missing CEPs were used in the analysis, the (relative) standard deviation would be even larger.

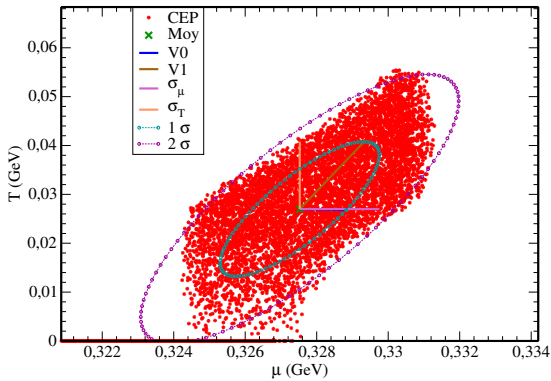[2] It is the characteristic crossover chemical potential at $T = 0$.

Figure 5. Scatter plot of the CEPs obtained for the uniform distribution of the input with a dispersion factor $p = 1\%$ and $n = 20^3$. Together with the data we display the position of the mean $(\mu_{\mathrm{CEP}}, T_{\mathrm{CEP}}) = (0.327, 0.026)$ (GeV) and the standard deviation $\sigma(T) = 0.019$ GeV and $\sigma(\mu) = 0.0076$ GeV. The $1-$ and $2-\sigma$ approximate confidence ellipses are shown also with the principal direction ($V_0 = 0.0013$ GeV and $V_1 = 0.0138$ GeV are eigenvectors of the covariance matrix of the data whose length is given by the square root of the corresponding eigenvalue). The confidence ellipses drawn at the $1-$ and $2-\sigma$ level are a convenient way to visualize the covariance matrix but there are not the true $1-$ and $2-\sigma$ confidence level. As the dispersion factor raises, the CEPs "disappear from bellow".
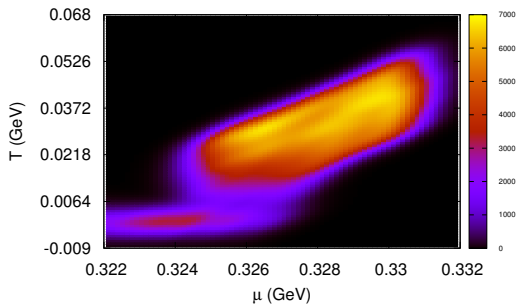

Figure 6. Kernel Density Estimate (KDE) of the CEP distribution probability in the same simulation condition as previously with $p = 1\%$ for the uniform density. The color coded z-axis is in GeV^{-2}. All parameter sets give rise to a data point (notice the points on the $T = 0$ line: if the CEP cannot be found it is replace by a $T = 0$ point (see text)).

3.2.4 Correlation of the chiral critical end points with the inputs

Finally, to better find how to constrain the model, it may be of interest to look at the correlations between the CEP coordinates and the phenomenological inputs (this has been shortly discussed in previous sections, for example when we studied variation of the CEP with respect to the condensate). The correlations between two quantities A and B that can be either inputs, parameters or predic-

tions may be accessed through the correlation coefficient C_{AB} defined as (see [34]):

$$C_{AB} = \frac{|\mathrm{Covar}(A, B)|}{\sigma(A)\sigma(B)} , \qquad (23)$$

where $\mathrm{Covar}(A, B)$ is the extra-diagonal coefficient of the covariance matrix of A and B. Explicitly, if A_i and B_i are the datasets generated by the Monte-Carlo, the covariance matrix elements are:

$$\mathrm{Covar}(A, B) = \frac{1}{n-1} \sum_{i=1}^{n} (A_i - \bar{A})(B_i - \bar{B}) \qquad (24)$$

($\bar{A}$ and $\bar{B}$ are the means of the corresponding dataset), $\mathrm{Covar}(B, A) = \mathrm{Covar}(A, B)$ and the diagonal elements are simply the variance *e.g.* $\mathrm{Covar}(A, A) = \sigma^2(A)$.

When this coefficient is close to one it means a strong correlation between A and B (for example C_{AA} is obviously equal to 1). On the contrary a value close to zero means that the random variable A and B are uncorrelated. To be precise, let us mention that the coefficient is a good measure of independence of a variable in the linear case; in the non-linear framework that we are working in, close to zero correlation may not imply that the two variables are almost independent. For this reason it is also important to check the conclusion one can infer from C_{AB} by inspecting the scatter plots of the datasets A and B (Fig. (7)). Since we start with a uniform distribution, perfect correlations will result in a line in the plot where the density of point is constant (and implies $C_{AB} = 1$) and no correlations will result in a rectangular shape where the density of points is also constant (and implies $C_{AB} = 0$).

We will concentrate on the correlations between the CEP coordinates and the phenomenological inputs or parameters. Indeed since the predictive power of the model is quite poor it is important to know which inputs or parameters should be better constrained to restore the robustness of the CEP prediction. On Fig. (7) we display correlation plots between the inputs and the CEP (temperature and chemical potential) with a dispersion of the inputs of 1% as in the previous plots. To complete this analysis, Tab. 5 puts together the values of the correlation coefficient Eq. (23) between the inputs or the parameters and the CEP coordinates.

We notice that the CEP position is almost uncorrelated to the value of m_π (another manifestation that the Goldstone theorem is a constraint strong enough to ensure that quantities not involving m_0 are largely insensitive to the precise mass of the pion) as can be seen on the plots (almost a perfect rectangular shape) or in the table (C is below 0.1 for both T and μ). Otherwise, there is a strong correlation of the CEP with f_π.

Let us stress that the plots are richer than the value of the coefficients. For example, we see that the "no CEP" points (represented as zero temperature points) correlates with low values of f_π or the condensate. The only difference between T and μ correlation coefficients with inputs concerns the condensate. The temperature is 4 times more correlated with it than the chemical potential. As already
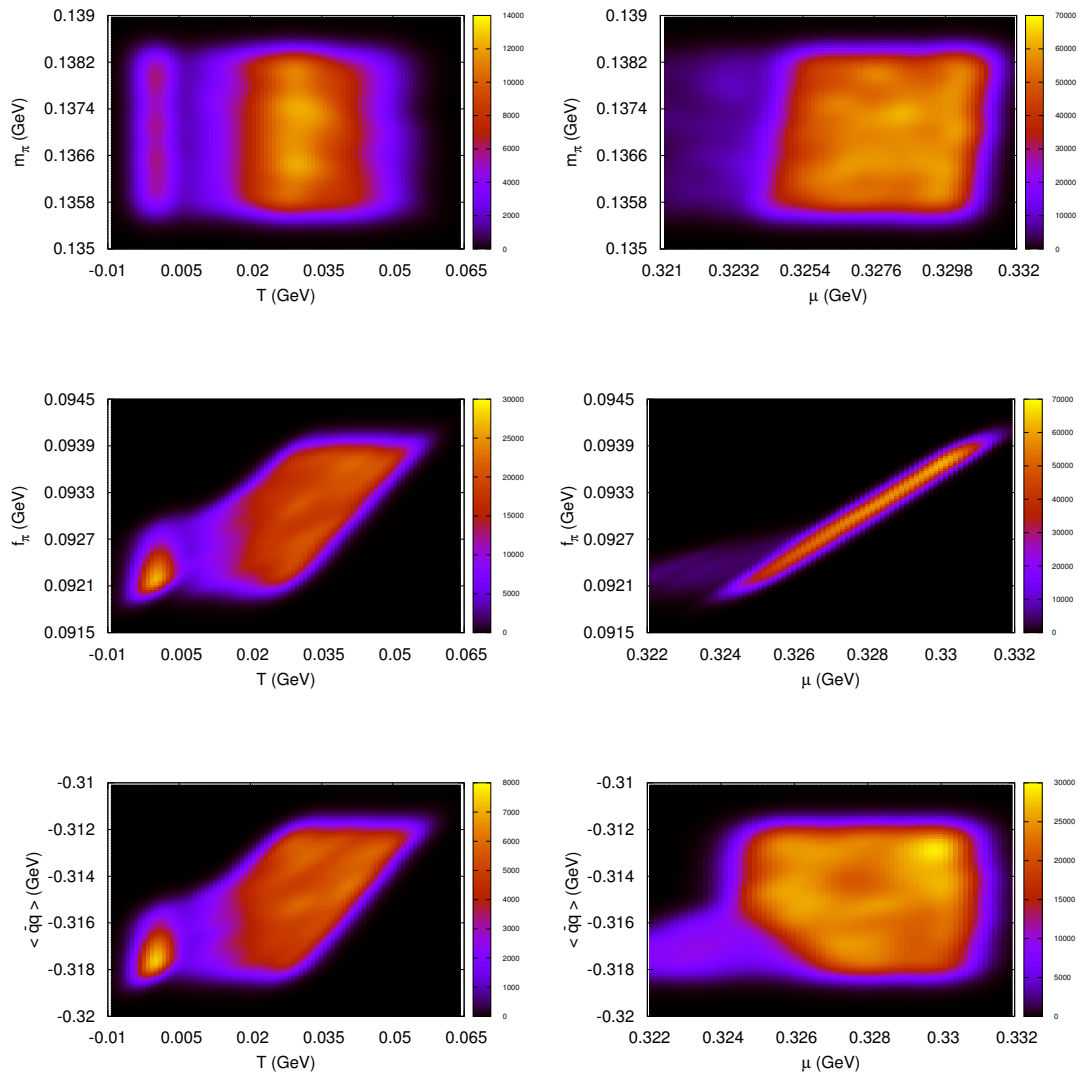
Figure 7. Correlation of the temperature (left) or the chemical potential (right) with the inputs. Uniform distribution, $p = 1\%$ MeV and $N = 20^3$. To represent the correlations we have done a scatter plot of the two datasets then reconstructed the density of points with the KDE algorithm App. (E). The color coded z-axis is then in GeV^{-2}.

mentioned, for the sigma mass and when we vary the condensate, this kind of relation could not have been easily found based on physical arguments, illustrating the power of the correlation analysis and the unexpected behavior of the inverse problem. This difference between T and μ correlations may be one of the reason why the temperature prediction is less robust (more dispersed) than the chemical potential one.

4 Conclusion

In this paper, the effects of infinitesimal variations of the inputs used to fix the parameters of the NJL model were systematically studied using the sensitivity parameter.

Correlations of		T_{CEP}	μ_{CEP}
with inputs	m_π	0.021	0.123
	f_π	0.646	0.987
	$\langle \bar{q}q \rangle$	0.591	0.130
with parameters	m_0	0.797	0.494
	Λ	0.933	0.445
	$G\Lambda^2$	0.975	0.686

Table 5. Correlation coefficients between the inputs or the model parameters with the temperature and the chemical potential at CEP with uniform distribution, $p = 1\%$, and $n = 20^3$.

This work is a benchmark for more realistic studies but we already shown how poorly the CEP temperature

is predicted by the model (if it can at all be predicted when considering finite variations).

The great advantage of the sensitivity is to quantitatively and systematically assess the information on how a quantity is reasonably predicted in a model without being obligated to vary by hand the value of the parameter to try to assess the stability of a prediction. Besides, the inverse problem analysis is done at constant vacuum phenomenology.

Along the way we have illustrated how powerful the tools from the inverse problem theory can be, revealing non trivial relations between inputs and predictions, for example when studying the sigma mass (whose physics is well understood within this model) or when softening the constraint on the condensate value (where we found a less trivial behavior).

The simulations requiring a large number of samples, we also show as an exercise in App. (A) an exact solution of the inverse problem and, App. (B), a fast algorithm to compute the CEP by pushing as much as possible the analytic calculation (in particular using no numerical derivatives that are known to be quickly badly behaved). In more realistic models, the former certainly won't be possible anymore, but our algorithm can be easily generalized.

The general conclusion is that with parameters fitted to the in-vacuum quantities, the intuition dictates that in-medium prediction may be less safe (even if it is the usual framework in the literature). What we have shown here is a way to give a quantitative statement about this intuition. We also show that for the case of the chemical potential it seems to go opposite to the intuition. With this work we suggest that for more realistic models such a sensitivity criterion (together with correlation analysis) may help to know in which direction the model should be refined and constrained to have better predictions.

One noticeable result that we will investigate further is that the chemical potential of the CEP is remarkably stable. Of course the vector interaction will change this value (the vector interaction essentially shifts the chemical potential) but we conjecture and we will check it in a next publication if the temperature still remains unpredictable.

From this remarkable stability we learn even with this simplified model that if the CEP is shown to exist (*e.g.* observationally if one has a proof that the transition is first order at zero temperature), the contribution of the scalar interaction will contribute to strongly constraint its chemical potential coordinate but the prediction of its temperature is not possible in this framework. It shows that one has to add other relevant physical mechanism for this prediction. We suppose that, in the PNJL model which add finite temperature constraints, this problem would be lessened (but not completely solved) since gluonic effect have an important role to fix the temperature.

We will also test if adding in medium inputs will indeed stabilize enough the prediction for it to be meaningful. The problem being of course that there is few finite density experimental/theoretical constraints to QCD. We will also study if even a very weak constraint (for example one coming from compact star phenomenology where experimental uncertainties are large) is able to stabilize the CEP and hence showing that effective models can be trust as a useful tool to study QCD where for example LQCD cannot reach.

Let us conclude on a more general note. The CEP position in this simple model is rather low in the phase diagram (small T, high μ), at the bottom of the chiral crossover and 1st order transition line. It may be related to the fact that its sensitivity is rather low: when varying parameters, the CEP essentially follows the transition line that is rather steep in this part of the phase diagram hence its value do not change a lot.

On the contrary LQCD or first experimental evidences [5] favor a much lower value of the chemical potential and a higher value of the temperature.

We already have shown [23] (Fig. 8) that with the SU(3) NJL model with a Polyakov loop (that take into account a static gauge field) the CEP is considerably higher in the phase diagram. We also shown that in order to put it even closer to the zero chemical potential axis (in better agreement with the aforementioned evidences) we must either force the strange mass to a very low, non-physical value (Fig. 8 of [23]) as it is well known (when all light quark masses are low the transition at zero chemical potential is first order) or impose a large value of the t'Hooft coupling constant (Fig. 9 of [23]) hence destroying the correct magnitude of the eta - eta' meson mass difference. If this evidences are confirmed it will be a priori difficult to get the correct position of the CEP with a correct description of the vacuum. It is the great advantage of this framework to be able to systematically study parametrization of the model that obey a given set of constraints (contrarily to the above mention work where we vary independently parameters without inspection of the induced phenomenology). In future works we will use these tools to check if a parametrization exists that can reproduce both reasonable vacuum mesonic spectrum and in-medium CEP position. If not, it may be an indication that some important effects are missing in the model either higher order correction, back reaction mechanism or even new mechanism absent of the model like dynamical contribution of the gluonic sector.

A NJL model and its analytic inversion

The NJL model we consider, whose Lagrangian is given by Eq. (1), has three parameters m_0, Λ and G that are fitted to the values of the pion mass, m_π, the pion decay constant f_π, and the quark condensate $\langle \bar{q}q \rangle$.

Let us recall the system of equations for the inverse problem we obtained in the text (Eq. (5), Eq. (6) and Eq. (4)). When $(m_\pi, f_\pi, \langle \bar{q}q \rangle)$ are fixed to their phenomenological values, one has to solved for the parameters Λ, m_0

and G the system:

$$m_\pi^2 = -\frac{m_0}{m}\frac{1}{4iGN_cN_fI_2(0)} , \qquad (25)$$

$$f_\pi^2 = -4iN_cm^2I_2(0) , \qquad (26)$$

$$\langle\bar{q}q\rangle = \frac{m_0 - m}{2G} , \qquad (27)$$

together with the equation for the mass m (Eq. (2)):

$$m_0 - m + 8iGN_cN_f mI_1 = 0 . \qquad (28)$$

A.1 Reduction of the system

The idea to reduce the system is to use adimensional quantities hence we conveniently rewrite Eq. (3) and Eq. (7):

$$I_1 = -i\Lambda^2 i_1(m/\Lambda),$$
$$\text{where } i_1(x) \equiv \int^1 \frac{d^3p}{(2\pi)^3}\frac{1}{2\sqrt{p^2+x^2}} , \qquad (29)$$

and

$$I_2(0) = \frac{i}{4}i_2(m/\Lambda),$$
$$\text{where } i_2(x) \equiv \int^1 \frac{d^3p}{(2\pi)^3}\frac{-1}{(p^2+x^2)^{3/2}} . \qquad (30)$$

The integrals i_1 and i_2 can be computed analytically:

$$i_1(x) = \frac{1}{8\pi^2}\left[\Lambda_E + x^2\log\left(\frac{x}{1+\Lambda_E}\right)\right] , \qquad (31)$$

$$i_2(x) = \frac{1}{2\pi^2}\left[\frac{1}{\Lambda_E} + \log\left(\frac{x}{1+\Lambda_E}\right)\right] , \qquad (32)$$

with $\Lambda_E = \sqrt{x^2+1}$.

To solve the system, the scale Λ is used to make the variables dimensionless:

$$x = m/\Lambda \quad \text{and} \quad x_0 = m_0/\Lambda$$

With these variables, the system reads:

$$\frac{m_\pi^2}{\Lambda^2} = \frac{x_0}{x}\frac{1}{G\Lambda^2 N_cN_f i_2(x)} , \qquad (33)$$

$$\frac{f_\pi^2}{\Lambda^2} = N_c x^2 i_2(x) , \qquad (34)$$

$$\frac{\langle\bar{q}q\rangle}{\Lambda^3} = \frac{x_0 - x}{2G\Lambda^2} , \qquad (35)$$

and the gap equation becomes:

$$0 = x_0 - x + 8G\Lambda^2 N_cN_f x i_1(x) . \qquad (36)$$

This equation is automatically solved if:

$$G\Lambda^2 = \frac{x - x_0}{8N_cN_f x i_1(x)} . \qquad (37)$$

This form for $G\Lambda^2$ can be plugged in Eq. (34) and Eq. (35). Introducing another new variable:

$$\delta = \frac{x - x_0}{x_0} ,$$

the system now reads:

$$\frac{m_\pi^2}{\Lambda^2} = \frac{8i_1(x)}{\delta i_2(x)} , \qquad (38)$$

$$\frac{f_\pi^2}{\Lambda^2} = N_c x^2 i_2(x) , \qquad (39)$$

$$\frac{\langle\bar{q}q\rangle}{\Lambda^3} = -4N_cN_f x i_1(x) . \qquad (40)$$

With this last form, we can solve it by first calculating the ratio:

$$\alpha = \frac{f_\pi^3}{\langle\bar{q}q\rangle}, \qquad (41)$$

which is a phenomenological constant independent of Λ and hence, by taking the quotient between Eq. (39) and Eq. (40), x is the solution of one equation of one unknown α:

$$G_\alpha(x) = 0 , \qquad (42)$$

with:

$$G_\alpha(x) = \frac{\sqrt{N_c}}{4N_f}\frac{x^2(i_2(x))^{3/2}}{i_1(x)} + \alpha . \qquad (43)$$

Once Eq. (42) is solved, we can compute δ by computing the ratio f_π^2/m_π^2 leading to:

$$\delta = \frac{f_\pi^2}{m_\pi^2}\frac{8i_1(x)}{N_c(x i_2(x))^2} . \qquad (44)$$

Finally, the system has just to be re-scaled:

$$\Lambda = \frac{f_\pi}{x\sqrt{N_c i_2(x)}} . \qquad (45)$$

The values of m_0 and G can now be calculated:

$$m_0 = \Lambda\frac{x}{\delta + 1} , \qquad (46)$$

$$G = \frac{1}{\Lambda^2}\frac{x - x_0}{8N_cN_f x i_1(x)} . \qquad (47)$$

A.2 Solution for x

Provided that none of the parameters is zero, the system given by Eqs. (38,39,40) is equivalent to Eq. (42)). This equation has to be solved for x, and depending on the value of α given Eq. (41), the system may be solved or not. In Fig. (8), the function G_α is plotted for three values of α. Calling x_{max} the abscissa such as G_α is maximum, then we see that Eq. (42) has solutions for each $\alpha > \alpha_c$, where α_c is defined as the α for which the value of the function G_α at x_{max} is zero:

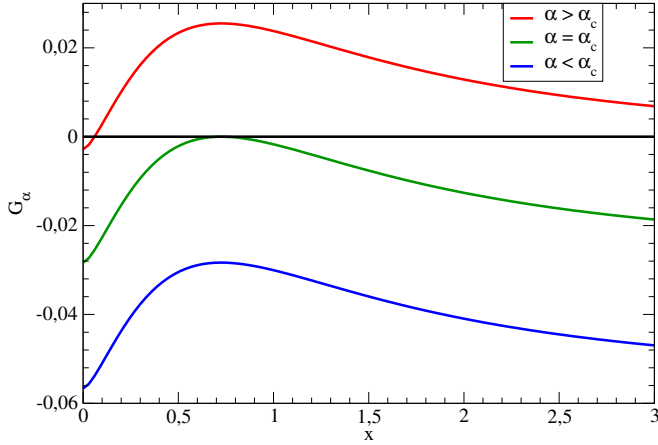$$\alpha_c \quad \Leftrightarrow \quad G_{\alpha_c}(x_{max}) = 0 . \qquad (48)$$

Figure 8. Function $G_\alpha(x)$ for three typical values of the parameter α (always negative for physical values of the phenomenological inputs):
(top) $0 > \alpha > \alpha_c$: two solutions; (middle) $\alpha = \alpha_c$: one degenerate solution at maximum; (bottom) $\alpha < \alpha_c$: no solution. If $\alpha > \alpha_c$ the system has two solutions: one is physical, for $x < x_{\max}$, while the other is not, for $x > x_{\max}$, where $x_{\max}$ is the abscissa of the maximum of G_α function.

Since the abscissa of the maximum value of $G_\alpha(x)$ is independent of α, the critical value is a numerical constant $\alpha_c = -0.0283275$ and has just to be calculated once. For all values of α that respect $\alpha > \alpha_c$ the system has two solutions. The first one is numerically found by any bracketing algorithm which is looking for a root in $[0, x_{\max}]$. This root corresponds to the physical dressed mass $x = m/\Lambda < x_{\max}$. The second root corresponds to an nonphysical mass $m/\Lambda > x_{\max}$ (it is another way to see the phenomenon described in [43], Fig. 2.6). Nevertheless, as a complement, we present a way to find it. It is possible to calculate an asymptote of $G_\alpha(x)$ at $x \to +\infty$ defined by:

$$G_\alpha^\infty(x) = \sqrt{\frac{N_c}{3}}\frac{x^{-3/2}}{4\pi N_f} + \alpha \;. \qquad (49)$$

The solution of $G_\alpha^\infty(x) = 0$ is analytic and reads:

$$x^\infty = -\left(\frac{N_c}{24}\right)^{1/3}(\alpha\pi N_f)^{-2/3} \;. \qquad (50)$$

The nonphysical root can be searched in the interval $[x_{\max}, x^\infty]$.

B Fast algorithm for the chiral critical end point calculation

To study the in-medium properties of the NJL model, one has to generalize the in-vacuum gap equation Eq. (28) for finite temperature and finite chemical potential. The gap equation to be solved is:

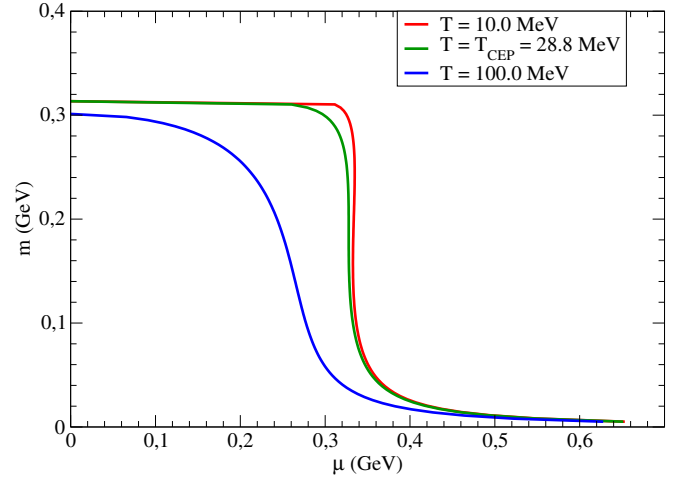$$g_m(m, T, \mu) = 0 \;, \qquad (51)$$

Figure 9. In medium dressed quark mass for the three typical cases described in text.

where:

$$g_m = m_0 - m + 8GN_cN_f m\left[iI_1(m, \Lambda) - I_\beta(m, T, \mu)\right] \;, \qquad (52)$$

with I_1 being the integral (29) and I_β the integral defined as:

$$I_\beta = \int^\infty \frac{d^3p}{(2\pi)^3}\frac{1}{2E_p}\left[f(p) + \bar{f}(p)\right] \;, \qquad (53)$$

where $E_p = \sqrt{p^2 + m^2}$ and f and $\bar{f}$ are the Fermi-Dirac distribution for quarks and antiquarks respectively

$$f(p) = \frac{1}{1 + \exp\left(\beta(E_p - \mu)\right)} \;,$$

$$\bar{f}(p) = \frac{1}{1 + \exp\left(\beta(E_p + \mu)\right)} \;,$$

with $\beta = T^{-1}$ and $k_B = 1$. The solution of Eq. (51) is plotted as a function of the chemical potential for different temperatures on Fig. (9). It displays three different behaviors:
(i) For $T > T_{\text{CEP}}$, there is a single solution $m(T, \mu)$ characteristic of a cross-over transition between a chirally broken hadronic phase ($\langle\bar{q}q\rangle \neq 0$) and an almost chirally symmetric phase ($\langle\bar{q}q\rangle \simeq 0$);
(ii) For $T < T_{\text{CEP}}$, it exists, in a range of chemical potential, three solutions for m, characteristic of a first order chiral phase transition with stable, metastable, and unstable solutions;
(iii) For $T = T_{\text{CEP}}$, it exists a unique solution m but if $\mu = \mu_{\text{CEP}}$, then the tangent of $m(T, \mu)$ is infinite: at the CEP, the phase transition is of second order.

Then, to compute the CEP coordinates, one has to compute the temperature and the chemical potential where m has a unique infinite tangent (strictly speaking one should work with the order parameter, namely the quark condensate, but it is equivalent and easier to work with the quark mass):

$$\left.\frac{dm}{d\mu}\right|_{T=T_{\text{CEP}}} = +\infty \quad \Leftrightarrow \quad \left.\frac{d\mu}{dm}\right|_{T=T_{\text{CEP}}} = 0 \;, \qquad (54)$$

where the function $\mu(m, T)$ is an implicit solution of $g_m(m, T, \mu(m, T)) = 0$ (this function is easier to work with since it is always single valued). Because of the unicity of the infinite tangent at the CEP, the latter is also an inflection point, meaning that finding the CEP coordinates means to solve the following system of equations:

$$g_m(m_{\mathrm{CEP}}, T_{\mathrm{CEP}}, \mu_{\mathrm{CEP}}) = 0 , \qquad (55)$$

$$\left.\frac{\mathrm{d}\mu}{\mathrm{d}m}\right|_T (m_{\mathrm{CEP}}, T_{\mathrm{CEP}}, \mu_{\mathrm{CEP}}) = 0 , \qquad (56)$$

$$\left.\frac{\mathrm{d}^2\mu}{\mathrm{d}m^2}\right|_T (m_{\mathrm{CEP}}, T_{\mathrm{CEP}}, \mu_{\mathrm{CEP}}) = 0 . \qquad (57)$$

The traditional way to compute the CEP is to solve numerically Eq. (55), then find the maximum of $\mathrm{d}\mu/\mathrm{d}m$ for any T, and then find T such as the value of $\mathrm{d}\mu/\mathrm{d}m$ at this temperature is zero. This method works quite well if the derivatives are not calculated numerically, and if adequate initial values are given to the algorithm. Using this method, the time required to compute the CEP position is a fraction of second. It the following we show how this calculation can be accelerated.

B.1 Rewriting of the gap equation

We introduce the new variables

$$\sigma = \beta\mu \qquad \text{and} \qquad x = \beta m .$$

Let us stress that the previous definition of the dimensionless parameters like the mass x was done with the scale Λ and now we use $1/\beta$: we keep the same name since there is no possibility of confusion. Renaming $p \to \beta p$ in the integral (53), we can write:

$$I_\beta(m, T, \mu) = T^2 i_\beta(\sigma, x) , \qquad (58)$$

where i_β is given by

$$i_\beta(\sigma, x) = \int^\infty \frac{\mathrm{d}^3 p}{(2\pi)^3} \frac{1}{2E} \left[f(p) + \bar{f}(p) \right] , \qquad (59)$$

with $E = \sqrt{p^2 + x^2}$, with f and $\bar{f}$ the Fermi-Dirac distributions $f = [1 + \exp(E \pm \sigma)]^{-1}$.

The mean field equation (55) can be rewritten using the new variables $x_0 = \beta m_0$, $\gamma = GT^2$, and $\lambda = \beta\Lambda$:

$$0 = x_0 - x - 8\gamma N_c N_f x \left[i_\beta(\sigma, x) - \lambda^2 i_1(x/\lambda) \right] . \qquad (60)$$

If one introduces the variable $\eta = x/\lambda$, then the previous equation can be written:

$$8\gamma N_c N_f \eta^2 i_1(\eta^{-1}) = 8\gamma N_c N_f \frac{i_\beta(\sigma, x)}{x^2} - \frac{x_0}{x^3} + x^{-2} . \qquad (61)$$

Using the definitions of the new variables, we can compute:

$$\frac{1}{\gamma x^2} = \frac{\eta^2}{G\Lambda^2} \quad \text{and} \quad \frac{x_0}{\gamma x^3} = \eta^3 \frac{m_0}{\Lambda} \frac{1}{G\Lambda^2} , \qquad (62)$$

and, introducing:

$$a = (8G\Lambda^2 N_c N_f)^{-1} \quad \text{and} \quad b = \frac{m_0}{\Lambda} , \qquad (63)$$

the mean field equation becomes:

$$a\eta^2(b\eta - 1) + \eta^2 i_1(\eta^{-1}) = \frac{i_\beta(\sigma, x)}{x^2} . \qquad (64)$$

We introduce the function $F(\eta)$:

$$F(\eta) = a\eta^2(b\eta - 1) + \eta^2 i_1(\eta^{-1}) , \qquad (65)$$

and the function $Z(\sigma, x)$:

$$Z(\sigma, x) = \frac{i_\beta(\sigma, x)}{x^2} , \qquad (66)$$

Such that Eq. (64) simply reads:

$$F(\eta) = Z(\sigma, x) . \qquad (67)$$

Since integral (59) is given by a numerical integral, calculating its inverse is time consuming. On the contrary $i_1(x)$ is analytical and $F^{-1}(\eta)$ can be efficiently computed with a simple root polishing algorithm without numerical integration. At fixed σ and x, the solution η of the mean field equation is:

$$\eta_{\mathrm{MFE}}(\sigma, x) = F^{-1} \circ Z(\sigma, x) , \qquad (68)$$

where η_{MFE} is then the η that solves the mean field equation, from which one can compute the mass, the temperature, and the chemical potential using:

$$m = \frac{\Lambda}{\eta_{\mathrm{MFE}}} ; \quad T = \frac{\Lambda}{x\eta_{\mathrm{MFE}}} ; \quad \mu = \frac{\Lambda\sigma}{x\eta_{\mathrm{MFE}}} . \qquad (69)$$

One may be surprised to work with these variables but, in fact, using these variables is equivalent to choose a trajectory on the surface defined by:

$$g_m(m, T, \mu) = 0 . \qquad (70)$$

For example, at fixed σ, computing $\eta(x)$ and then $m(x) = \Lambda/\eta(x)$ is equivalent to compute $g_m(m, T, \mu) = 0$ with the constraints $\sigma = \mathrm{cst} = \mu/T$.

The parametric curve $\{m = m(x) , \mu = \Lambda\sigma/[x\eta(x)]\}$ at σ fixed is simply the solution of:

$$g_m\left(m(\mu), T = \frac{\mu}{\sigma}, \mu\right) = 0 , \qquad (71)$$

i.e., it is the solution of the mean field equation on lines $T = \mu/\sigma$ in the (T, μ) plane.

We have to be careful in the following since the CEP is defined as the point where m has an infinite derivative with respect to the thermodynamical parameters T and μ. In the light of Eq. (71), computing the CEP coordinates is equivalent to solve the system given by Eqs. (55,56,57) at a fixed σ. As a remark we notice that working at fixed x gives simpler equations but one can check that the solution found will not be the CEP. Indeed the trajectory followed on the surface $S = \{g_m(m, T, \mu) = 0\}$ is not trivial and the link between this solution and the CEP is not obvious.

B.2 Finding the CEP

Using the previous notations, the system can be rewritten as:

$$F(\eta) = Z(\sigma, x) \ , \tag{72}$$

$$\left.\frac{\mathrm{d}\mu}{\mathrm{d}m}\right|_\sigma = 0 \ , \tag{73}$$

$$\left.\frac{\mathrm{d}^2\mu}{\mathrm{d}m^2}\right|_\sigma = 0 \ , \tag{74}$$

where

$$\frac{\mu}{\Lambda}(\sigma, x) = \frac{\sigma}{\eta x} \ , \tag{75}$$

$$\frac{m}{\Lambda}(\sigma, x) = \eta^{-1} \ . \tag{76}$$

At fixed σ, we can compute the total differentials:

$$\mathrm{d}\left(\frac{\mu}{\Lambda}\right) = -\frac{\sigma}{x\eta^2}\mathrm{d}\eta - \frac{\sigma}{\eta x^2}\mathrm{d}x \ , \tag{77}$$

$$\mathrm{d}\left(\frac{m}{\Lambda}\right) = -\frac{\mathrm{d}\eta}{\eta^2} \ . \tag{78}$$

From Eq. (72), and using Eq. (77) and Eq. (78) we have:

$$\eta F'(\eta) + x Z_x(\sigma, x) = 0 \ , \tag{79}$$

where F' is the derivative of F with respect to η, and Z_x is the partial derivative of Z with respect to x.

In the same fashion, we can write:

$$0 = \left.\frac{\mathrm{d}^2\mu}{\mathrm{d}m^2}\right|_\sigma$$
$$= \frac{\mathrm{d}}{\mathrm{d}m}\left[-\frac{\sigma}{\eta x}\left(\eta^{-1} + x^{-1}\frac{\mathrm{d}x}{\mathrm{d}\eta}\right)(-\eta^2)\right] \ . \tag{80}$$

After some manipulations, and using Eq. (79), one finds:

$$\eta^2 F''(\eta) - x^2 Z_{xx}(\sigma, x) - 2x Z_x(\sigma, x) = 0 \ , \tag{81}$$

where Z_{xx} is the second partial derivative of Z with respect to x.

The system to solve is now:

$$F(\eta) - Z(\sigma, x) = 0 \ , \tag{82}$$

$$\eta F'(\eta) + x Z_x(\sigma, x) = 0 \ , \tag{83}$$

$$\eta^2 F''(\eta) - x^2 Z_{xx}(\sigma, x) - 2x Z_x(\sigma, x) = 0 \ . \tag{84}$$

With the correct initialization, in particular if the initialization for η is already the solution of Eq. (68) for the initial values of x and σ, a simple root finding algorithm can compute the solution in a few millisecond (this algorithm is about a hundred times faster than the usual algorithm).

Depending on a and b Eq. (63), the CEP may disappear. In that case, one should not try to solve the system given by Eqs. (82,83,84). To detect if the CEP exists, it is always equivalent to have a metastable solution at zero temperature. Hence, by solving $\mathrm{d}^2\mu/\mathrm{d}^2m = 0$, and looking at the value of $\mathrm{d}\mu/\mathrm{d}m$ at this point, one can very efficiently (also a few millisecond) determine if the CEP exists ($\mathrm{d}\mu/\mathrm{d}m > 0$) or not.

C Analytical derivation of the sigma-meson mass sensitivity

To compute the sensitivity in the case of the sigma-meson mass:

$$m_\sigma^2 = 4m^2 + m_\pi^2 \ , \tag{85}$$

one can use the previous change of variable $m = \Lambda x$ and then:

$$m_\sigma^2 = 4\Lambda^2 x^2 + m_\pi^2 \ . \tag{86}$$

If x is solution of Eq. (42), then Λ is given by Eq. (45), and the sigma meson mass reads:

$$m_\sigma = \sqrt{\frac{4}{N_c}\frac{f_\pi^2}{i_2} + m_\pi^2} \ . \tag{87}$$

With $c^3 = -\langle \bar{q}q \rangle$ we have the differential:

$$di_2 = \frac{di_2}{dx}dx = -\frac{di_2}{dx}\frac{1}{G'_\alpha(x)}d(f_\pi^3/c^3). \tag{88}$$

It is straightforward to compute $\mathrm{d}m_\sigma^2 = 2m_\sigma \mathrm{d}m_\sigma$ and finally the needed partial derivatives. We found:

$$\frac{\partial m_\sigma}{\partial m_\pi} = \frac{m_\pi}{m_\sigma} \ , \tag{89}$$

$$\frac{\partial m_\sigma}{\partial f_\pi} = \frac{2f_\pi}{m_\sigma N_c i_2}\left(2 + \frac{3\alpha}{i_2}\frac{di_2}{dx}\frac{1}{G'_\alpha}\right) \ , \tag{90}$$

$$\frac{\partial m_\sigma}{\partial c} = -6\frac{f_\pi^2}{m_\sigma N_c i_2^2}\frac{\alpha}{c}\frac{di_2}{dx}\frac{1}{G'_\alpha} \ . \tag{91}$$

With the value of the inputs in the manuscript one finds: $\mathrm{d}m_\sigma = 0.21\mathrm{d}m_\pi + 34\mathrm{d}f_\pi - 8.2\mathrm{d}c$ so, for a vanishing relative dispersion, $\Sigma(m_\sigma) = 6.42$. The value we obtained with the Monte-Carlo, Tab. 1, is $\Sigma(m_\sigma) = 6.41$.

The (small) difficulty here comes from the implicit equation for x. In this particular case, all the quantities that appear in the inverse problem only depend on the solution of Eq. (42) which only depends on the quantity $\alpha = f_\pi^3/c^3$, and then one can access the sensitivity of the in-vacuum predictions quite easily. With more realistic models, the inverse problem will not be equivalent anymore to a one dimensional equation, and the Monte Carlo becomes a better alternative.

D Analytical calculation of composed probability distributions

To check if the Monte-Carlo results are correct, one can compare them to the theoretical probability distributions when possible.

In the one variable case, the composition of two probability distributions is as follow. Let's call X and Y two random variables, with X following its probability distribution ρ_X, and $Y = f(X)$ (i.e. Y is a function of the random variable X). Let's call x and y the realization of

the random variables X and Y through their corresponding probability distributions.

If the function f is monotonic and increasing, then the probability of finding x between x_1 and x_2 ($x_1 < x_2$) is equal to the probability of finding y between $y_1 = f(x_1)$ and $y_2 = f(x_2)$:

$$P(x_1 \leq x \leq x_2) = P(y_1 = f(x_1) \leq y \leq y_2 = f(x_2)) . \tag{92}$$

By definition of the probability distribution we have:

$$P(x_1 \leq x \leq x_2) = \int_{x_1}^{x_2} \rho_X(x)\mathrm{d}x ; \tag{93}$$

$$P(y_1 \leq y \leq y_2) = \int_{f(x_1)}^{f(x_2)} \rho_Y(x)\mathrm{d}y . \tag{94}$$

Then ρ_X can be expressed as:

$$\rho_X(x) = (\rho_Y \circ f)(x)f'(x) , \tag{95}$$

which imply:

$$\rho_Y(y) = \left(\rho_X \circ f^{-1}\right)(y) \left[\left(f' \circ f^{-1}\right)(y)\right]^{-1} . \tag{96}$$

To illustrate the case of two variables, we give the result for the density ρ_α. We have, following the same treatment as for the one variable case, and using the shortcuts f for f_π, and c for $\langle \bar{q}q \rangle$:

$$
\begin{aligned}
P(\alpha_1 \leq \alpha \leq \alpha_2) &= P\left(\frac{f^3}{c} \in [\alpha_1, \alpha_2]\right) \\
&= P\left(\frac{f^3}{c} \geq \alpha_1 \;\wedge\; \frac{f^3}{c} \leq \alpha_2\right) \\
&= P\left(f \in \mathbb{R}^+ \;\wedge\; \frac{f^3}{\alpha_2} \leq x \leq \frac{f^3}{\alpha_1}\right) \\
&= \int_{\mathbb{R}^+} \mathrm{d}f \int_{f^3/\alpha_2}^{f^3/\alpha_1} \mathrm{d}c \, \rho_f(f)\rho_c(c) . \tag{97}
\end{aligned}
$$

This probability can be re-expressed using the probability distribution ρ_α:

$$P(\alpha_1 \leq \alpha \leq \alpha_2) = \int_{\alpha_1}^{\alpha_2} \rho_\alpha(\alpha)\mathrm{d}\alpha , \tag{98}$$

and then we find an expression for ρ_α:

$$\rho_\alpha(\alpha) = \frac{\mathrm{d}}{\mathrm{d}\alpha} \int_{\mathbb{R}^+} \mathrm{d}f \int_{f^3/\alpha}^{f^3/\alpha^*} \mathrm{d}c \, \rho_f(f)\rho_c(c) , \tag{99}$$

where α^* is any constant. Finally ρ_α is found to read:

$$\rho_\alpha(\alpha) = \frac{1}{\alpha^2} \int_{\mathbb{R}^+} \mathrm{d}f \, f^3 \rho_f(f)\rho_c(f^3/\alpha) . \tag{100}$$

E Kernel density approximation

The statistical technique we used allowed us to draw some scatter plots for the CEP coordinates prediction. It is also interesting to have access to the probability distribution of the CEP, *i.e.* the density of points, in the $(T - \mu)$ plane. In order to reconstruct the density from the data, a possibility is to use the Kernel Density Estimate (KDE) with Gaussian kernels.

Following Eqs.(4), (5), (6) and (7) of [52] we can reconstruct the density $\rho(T_{CEP}, \mu_{CEP})$. This algorithm normalizes the density to get a probability distribution ($\int \rho(T, \mu)\, dT\, d\mu = 1$) hence its dimension is GeV^{-2}. To do this:

First we compute the covariance matrix and transform the data to obtain a set of data with zero mean value and unity standard deviation – the so-called sphered data. One has simply to apply to data the matrix $S^{1/2}$ where S is the covariance matrix.

Then each sphered data point is replaced by a Gaussian with a variance chosen such as its standard deviation is large enough to overlap with other data points but small enough not to create a long tail that does not exist in data. This is the smoothing procedure control by the smoothing parameter h of Hwang. We check that with the parameter h given in the paper, we are able to reconstruct very well a two dimensional Gaussian distribution with as low as a hundred point (it is the "easy case" for this algorithm) but also to reconstruct quite well a 2D uniform distribution also with a hundred points (the difficult case).

Finally the reconstructed density is the sum of the smoothed sphered data where the matrix $S^{-1/2}$ is applied to get back to the original data.

References

1. M. Asakawa and K. Yazaki. Chiral Restoration at Finite Density and Temperature. Nucl.Phys., A504:668–684, 1989.
2. B.I. Abelev et al. Identified particle production, azimuthal anisotropy, and interferometry measurements in Au+Au collisions at s(NN)**(1/2) = 9.2- GeV. Phys.Rev., C81:024911, 2010.
3. M.M. Aggarwal et al. An Experimental Exploration of the QCD Phase Diagram: The Search for the Critical Point and the Onset of De-confinement. 2010.
4. Terence J. Tarnowsky. Searching for the QCD Critical Point Using Particle Ratio Fluctuations and Higher Moments of Multiplicity Distributions. J.Phys., G38:124054, 2011.
5. Roy A. Lacey. Indications for a Critical End Point in the Phase Diagram for Hot and Dense Nuclear Matter. Phys.Rev.Lett., 114(14):142301, 2015.
6. Yasuyuki Akiba, Aaron Angerami, Helen Caines, Anthony Frawley, Ulrich Heinz, et al. The Hot QCD White Paper: Exploring the Phases of QCD at RHIC and the LHC. 2015.
7. 8th International Workshop on Critical Point and Onset of Deconfinement, 2013.
8. Xiaofeng Luo, Ming Shao, Cheng Li, and Hongfang Chen. Signature of QCD critical point: Anomalous transverse velocity dependence of antiproton-proton ratio. Phys.Lett., B673:268–271, 2009.
9. Rajiv V. Gavai. QCD Critical Point: Synergy of Lattice and Experiments. Acta Phys.Polon., B43:723–730, 2012.

10. Marek Gazdzicki. NA49/NA61: results and plans on beam energy and system size scan at the CERN SPS. J.Phys., G38:124024, 2011.

11. D. Blaschke et al. Searching for for a QCD Mixed Phase at the Nuclotron-Based Ion Collider Facility (NICA White Paper). Dubna, 2013.

12. Z. Fodor and S.D. Katz. Critical point of QCD at finite T and mu, lattice results for physical quark masses. JHEP, 0404:050, 2004.

13. Szabolcs Borsanyi, Gergely Endrodi, Zoltan Fodor, Antal Jakovac, Sandor D. Katz, et al. The QCD equation of state with dynamical quarks. JHEP, 1011:077, 2010.

14. A. Bazavov, T. Bhattacharya, M. Cheng, C. DeTar, H.T. Ding, et al. The chiral and deconfinement aspects of the QCD transition. Phys.Rev., D85:054503, 2012.

15. K. Fukushima. Chiral effective model with the polyakov loop. Physics Letters B, 591:277–284, 2004.

16. C. Ratti, M.A. Thaler, and W. Weise. Phases of QCD: Lattice thermodynamics and a field theoretical model. Physical Review D, 73(014019), 2006.

17. Pedro Costa, C.A. de Sousa, M.C. Ruivo, and Yu.L. Kalinovsky. The QCD critical end point in the SU(3) Nambu-Jona-Lasinio model. Phys.Lett., B647:431–435, 2007.

18. K. Fukushima. Phase diagrams in the three-flavor nambu jona-lasinio model with the polyakov loop. Physical Review D, 77(114028), 2008.

19. K. Kashiwa, H. Kouno, M. Matsuzaki, and M. Yahiro. Critical endpoint in the polyakov loop extended njl model. Physics Letters B, 662:26–32, 2008.

20. S. Rossner, T. Hell, C. Ratti, and W. Weise. The chiral and deconfinement crossover transitions: Pnjl model beyond mean field. Nuclear Physics A, 814:118–143, 2008.

21. Pedro Costa, C.A. de Sousa, M.C. Ruivo, and H. Hansen. The QCD critical end point in the PNJL model. Europhys.Lett., 86:31001, 2009.

22. P. Costa, H. Hansen, M. C. Ruivo, and C. A. de Sousa. How parameters and regularization affect the polyakov–nambu–jona-lasinio model phase diagram and thermodynamic quantities. Phys. Rev. D, 81:016007, Jan 2010.

23. Pedro Costa, M.C. Ruivo, C.A. de Sousa, and H. Hansen. Phase diagram and critical properties within an effective model of QCD: the Nambu-Jona-Lasinio model coupled to the Polyakov loop. Symmetry, 2:1338–1374, 2010.

24. Bernd-Jochen Schaefer, Jan M. Pawlowski, and Jochen Wambach. The Phase Structure of the Polyakov–Quark-Meson Model. Phys.Rev., D76:074023, 2007.

25. Tina Katharina Herbst, Jan M. Pawlowski, and Bernd-Jochen Schaefer. The phase structure of the Polyakov–quark-meson model beyond mean field. Phys.Lett., B696:58–67, 2011.

26. Kenji Fukushima. Phase diagrams in the three-flavor Nambu-Jona-Lasinio model with the Polyakov loop. Phys.Rev., D77:114028, 2008.

27. Nino M. Bratovic, Tetsuo Hatsuda, and Wolfram Weise. Role of Vector Interaction and Axial Anomaly in the PNJL Modeling of the QCD Phase Diagram. Phys.Lett., B719:131–135, 2013.

28. G.A. Contrera, A.G. Grunfeld, and D.B. Blaschke. Phase diagrams in nonlocal PNJL models constrained by Lattice QCD results. 2012.

29. Thomas Hell, Kouji Kashiwa, and Wolfram Weise. Impact of vector-current interactions on the QCD phase diagram. J.Mod.Phys., 4:644–650, 2013.

30. O. Kaczmarek, F. Karsch, E. Laermann, C. Miao, S. Mukherjee, et al. Phase boundary for the chiral transition in (2+1) -flavor QCD at small values of the chemical potential. Phys.Rev., D83:014504, 2011.

31. David Blaschke, David E. Alvarez-Castillo, and Sanjin Benic. Mass-radius constraints for compact stars and a critical endpoint. PoS, CPOD2013:063, 2013.

32. Albert Tarantola. Inverse Problem Theory and Methods for Model Parameter Estimation. Society for Industrial and Applied Mathematics, 2005.

33. A.G. Ramm. Inverse problems, tomography, and image processing. Springer, 1997.

34. J. Dobaczewski, W. Nazarewicz, and P.-G. Reinhard. Error Estimates of Theoretical Models: a Guide. J.Phys., G41:074001, 2014.

35. J. Toivanen, J. Dobaczewski, M. Kortelainen, and K. Mizuyama. Error analysis of nuclear mass fits. Phys. Rev. C, 78:034306, Sep 2008.

36. P.G. Reinhard and W. Nazarewicz. Information content of a new observable: The case of the nuclear neutron skin. Phys.Rev.C, 81(051303(R)), 2010.

37. F.J. Fattoyev and J. Piekarewicz. Accurate calibration of relativistic mean-field models: Correlating observables and providing meaningful theoretical uncertainties. Phys.Rev.C, 84(064302), 2010.

38. M. Kortelainen, T. Lesinski, J. More, W. Nazarewicz, J. Sarich, et al. Nuclear Energy Density Optimization. Phys.Rev., C82:024313, 2010.

39. Mario Wschebor Felipe Cucker. On the expected condition number of linear programming problems. NumerischeMathematik, 2002.

40. J.W. Demmel. On condition numbers and the distance of the nearest ill-pose problem. Numerische Mathematik, 51:251, 1987.

41. S. P. Klevansky. The Nambu—Jona-Lasinio model of quantum chromodynamics. Rev. Mod. Phys., 64:649–708, Jul 1992.

42. U. Vogl and W. Weise. The Nambu and Jona-Lasinio model: Its implications for Hadrons and Nuclei. Progress in Particle and Nuclear Physics, 27(0):195 – 272, 1991.

43. Michael Buballa. NJL-model analysis of dense quark matter. Physics Reports, 407(4–6):205 – 376, 2005.

44. Tetsuo Hatsuda and Teiji Kunihiro. QCD phenomenology based on a chiral effective lagrangian. Physics Reports, 247(5–6):221 – 367, 1994.

45. H.G. Dosch and S. Narison. Direct extraction of the chiral quark condensate and bounds on the light quark masses. Physics Letters B, 417(1–2):173 – 176, 1998.

46. J. Bordes, C.A. Dominguez, P. Moodley, J. Peñarrocha, and K. Schilcher. Chiral corrections to the su(2)xsu(2) gell-mann-oakes-renner relation. Journal of High Energy Physics, 2010(5), 2010.

47. Sinya Aoki, Yasumichi Aoki, Claude Bernard, Tom Blum, Gilberto Colangelo, et al. Review of lattice results concerning low energy particle physics. arXiv, 1310.8555, 2013.

48. O. Lourenco, M. Dutra, T. Frederico, A. Delfino, and M. Malheiro. Vector interaction strength in Polyakov-Nambu-Jona-Lasinio models from hadron-quark phase diagrams. Phys.Rev., D85:097504, 2012.

49. Micaela Oertel. Investigation of meson loop effects in the Nambu-Jona-Lasinio model. doctoral dissertation arXiv: hep-ph/0012224, 2000.

50. L.S. Celenza, Shun-fu Gao, Bo Huang, Huangsheng Wang, and C.M. Shakin. Covariant confinement model for the calculation of the properties of scalar mesons. Phys.Rev., C61:035201, 2000.

51. L. S. Celenza, Huangsheng Wang, and C. M. Shakin. Application of a generalized Nambu-Jona-Lasinio model to the calculation of the properties of scalar mesons and nuclear matter. Phys.Rev., C63:025209, 2001.

52. Jenq-Neng Hwang, S.-R. Lay, and A Lippman. Nonparametric multivariate density estimation: a comparative study. Signal Processing, IEEE Transactions on, 42(10):2795–2810, Oct 1994.